Tmem263 deletion disrupts the GH/IGF-1 axis and causes dwarfism and impairs skeletal acquisition

Dylan C. Sarver[1], Jean Garcia-Diaz[2,3,4], Ryan C. Riddle[2,4,5], G. William Wong[1]

Affiliations:

[1]Department of Physiology, Johns Hopkins University School of Medicine, Baltimore, Maryland, USA

[2]Department of Orthopaedic Surgery, Johns Hopkins University School of Medicine, Baltimore, Maryland, USA

[3]Department of Orthopaedics, University of Maryland School of Medicine, Baltimore, Maryland, USA

[4]Cell and Molecular Medicine graduate program, Johns Hopkins University School of Medicine, Baltimore, Maryland, USA

[5]Research and Development Service, Baltimore Veterans Administration Medical Center, Baltimore, Maryland, USA

Running head: TMEM263 inactivation results in Laron-type dwarfism

Corresponding author: G. William Wong, E-mail: gwwong@jhmi.edu, Department of Physiology, Johns Hopkins University School of Medicine, Baltimore, MD 21205

Tel: 410-502-4862

Fax: 410-614-8033

ABSTRACT

Genome-wide association studies (GWAS) have identified a large number of candidate genes believed to affect longitudinal bone growth and bone mass. One of these candidate genes, *TMEM263*, encodes a poorly characterized plasma membrane protein. Single nucleotide polymorphisms in TMEM263 are associated with bone mineral density in humans and mutations are associated with dwarfism in chicken and severe skeletal dysplasia in at least one human fetus. Whether this genotype-phenotype relationship is causal, however, remains unclear. Here, we determine whether and how TMEM263 is required for postnatal growth. Deletion of the *Tmem263* gene in mice causes severe postnatal growth failure, proportional dwarfism, and impaired skeletal acquisition. Mice lacking Tmem263 show no differences in body weight within the first two weeks of postnatal life. However, by P21 there is a dramatic growth deficit due to a disrupted GH/IGF-1 axis, which is critical for longitudinal bone growth. *Tmem263*-null mice have low circulating IGF-1 levels and pronounced reductions in bone mass and growth plate length. The low serum IGF-1 in *Tmem263*-null mice is due to a deficit in hepatic GH receptor (GHR) expression and GH-induced JAK2/STAT5 signaling. Consequently, Tmem263 loss-of-function results in GH insensitivity (GHI), and a dramatic alteration in the GH-regulated transcriptome in liver. Our data validates the causal role for Tmem263 in regulating postnatal growth and raises the possibility that rare mutations or variants of *TMEM263* may potentially cause GHI and impair linear growth.

Key words: Laron dwarfism, skeletal dysplasia, growth hormone, IGF-1, GHR, growth hormone insensitivity

INTRODUCTION

Skeletal development, growth, and the maintenance of tissue structure and mass across the lifespan are regulated by complex interactions between genetics and environment. A better understanding of these interactions and how they influence the function of cells responsible for skeletal homeostasis will provide actionable targets to mitigate skeletal disease. In exploring the heritability of bone growth and mass, genome wide association studies have identified large number of potential genes associated with bone mineral density (BMD) (1, 2), bone structure (3, 4) and height (5). However, it remains a daunting challenge to prioritize and establish the causal role for these candidate genes. Consequently, only a limited number of the GWAS candidate genes have been functionally validated to play a causal role.

TMEM263, also referred to as C12orf23, was identified through associations between femoral neck BMD and heel bone BMD (1, 2). Its function is unknown, but subsequent gene network analysis placed TMEM263 in a module related to osteoblast function (6). Intriguingly, a non-sense mutation (Trp59*) that truncate the TMEM263 protein is linked to dwarfism in chicken (7), although it is unclear if this mutation directly causes dwarfism. More recently, a two nucleotide deletion that causes a frameshift and premature termination in *TMEM263* was implicated as a candidate gene for a severe case of autosomal recessive skeletal dysplasia in a fetus (8). Apart from this limited information, little is known about TMEM263 and its function.

It is known that the growth hormone (GH) and Insulin-like growth factor 1 (IGF-1) axis plays a critical and essential role in postnatal growth (9-14). Defect in any component of this axis causes a variable spectrum (modest to severe) of growth retardation and skeletal dysplasia in humans and in animal models (15-27). Since mutation in *TMEM263* is linked to human skeletal dysplasia and dwarfism in chicken, and *TMEM263* is also a GWAS candidate gene for BMD, we speculated that TMEM263 may be a novel regulator of the GH/IGF-1 axis. We therefore set out to test this hypothesis using a genetic approach.

We showed here that Tmem263 is not required for embryonic development, prenatal growth, and fertility. However, mice lacking Tmem263 exhibit growth arrest and have severe reduction in bone mass and growth plate length. We

further showed that these defects are due to a marked reduction in GH receptor (Ghr) mRNA and protein expression in the liver. This resulted in greatly diminished GH-induced JAK2/STAT5 signaling critical for IGF-1 synthesis and secretion by the liver. Consequently, *Tmem263* knockout (KO) mice had low circulating IGF-1 and IGFBP3, leading to dramatic postnatal growth failure and skeletal dysplasia. Our loss-of-function studies have provided direct evidence that Tmem263 is a causal gene affecting BMD and postnatal growth, and it does so by regulating the GH/IGF-1 axis, specifically hepatic GHR protein levels. The GH insensitivity (GHI) phenotype seen in *Tmem263*-KO mice raises the intriguing possibility that rare *TMEM263* mutations or variants may potentially disrupt postnatal linear growth due to deficiency in GHR signaling.

RESULTS

TMEM263 is a conserved and widely expressed plasma membrane protein

The human *TMEM263* gene encodes a small protein of 116 amino acids with two predicted transmembrane helices (Fig. 1A). It is highly conserved across vertebrate species, with the fish (*Danio rerio*), frog (*Xenopus tropicalis*), chicken (*Gallus gallus*), and mouse (*Mus musculus*) orthologs sharing 73, 77, 90, and 97% amino acid identity with the full-length human TMEM263. In humans, the *TMEM263* transcript is widely and variably expressed across tissues (Fig. 1B), with liver having the highest expression. The expression data is based on the consensus dataset of normalized expression (nTPM) levels across tissues by combining the Human Protein Atlas (HPA) (28) and Gene-Tissue Expression (GTEx) transcriptomics datasets (29). Reflecting the transcript expression profile, human TMEM263 protein is also widely expressed (www.proteinatlas.org) (28). The mouse *Tmem263* is also variably and widely expressed across tissues (Fig. 1C).

Human TMEM263 protein is ~20 kDa in size when expressed in mammalian HEK293 cells (Fig. 1D). The presence of two putative hydrophobic segments suggests that TMEM263 may be an integral membrane protein. However, different transmembrane prediction programs have given inconsistent results. To experimentally determine whether human TMEM263 is a membrane protein localized to the cell surface or other intracellular membrane compartments, we performed surface biotinylation followed by streptavidin pull-down and immunoblot analysis. The

cell-impermeable biotinylation reagent labeled only proteins on the surface of intact cells. This analysis showed that TMEM263 is localized to the plasma membrane when expressed in HEK293 cells (Fig. 1E).

Tmem263 is not required for development and prenatal growth

A genetic approach was used to determine the *in vivo* function of Tmem263. The mouse *Tmem263* gene (NM_001013028) consists of three exons, and exon 3 encodes ~81% of the full-length protein. To generate a loss-of-function mouse model, we used CRISPR/Cas9 method to delete the entire protein-coding portion of exon 3, thus ensuring a complete null allele (Fig. 2A). We performed genomic PCR and DNA sequencing to confirm the genotype and deletion of the *Tmem263* gene (Fig. 2A-B). As expected, deletion of the *Tmem263* gene resulted in complete absence of the transcript in liver and hypothalamus (Fig. 2C).

The genotype distribution of 82 pups at postnatal day 1 (P1) largely conformed to the expected Mendelian ratio for WT (+/+), heterozygous (+/-), and KO (-/-) mice (Fig. 2D), indicating that Tmem263 is not required for embryonic development. Loss of Tmem263 did not affect suckling at P1, as the milk spot was clearly visible in *Tmem263*-KO pups (Fig. 2E). No gross anatomical abnormalities in the axial skeleton, appendages, and cartilage were noted in *Tmem263*-KO pups at P1, indicating that Tmem263-KO mice were born normal (Fig. 2F). The birth weights of pups at P1 were also not different between genotypes (Fig. 2G). Together, these data indicate that Tmem263 is not required for embryonic development and prenatal growth.

Tmem263 deletion causes severe postnatal growth retardation

From P1 to P14, the weights of *Tmem263*-KO pups were not different from WT controls (Fig. 2G), indicating no deficit in growth trajectory within the first two weeks of life. However, before and around the time of weaning at P21 when mice started to experience an accelerated growth spurt, coincident with the initiation of GH action (15), clear differences in body weight were noted in *Tmem263*-KO mice relative to WT (+/+) and heterozygous (+/-) controls (Fig. 2G). By adulthood (8 weeks old), a severe growth failure phenotype was apparent in the *Tmem263*-KO mice (Fig. 2H).

Both male and female KO mice exhibited the same striking degree of dwarfism, with body weight and body length dramatically reduced relative to WT controls (Fig. 2I-K). Due to their small size, the organ weights (liver, pancreas, heart, kidney, spleen, gastrocnemius, and brain) of the KO mice were significantly lower relative to WT

controls (Figure 2-figure supplement 1). When normalized to their body weight, *Tmem263*-KO mice also had lower relative weights of liver (male only), spleen (male only), and skeletal muscle (gastrocnemius) and higher kidney and brain weight (Figure 2-figure supplement 1). Partial loss of *Tmem263* did not result in haploid insufficiency, as the heterozygous (+/-) mice were indistinguishable from WT littermates across all measured parameters. Both male and female *Tmem263*-KO mice were fertile, as indicated by viable mouse litters derived from multiple independent matings between male (-/-) and female (-/-) mice. The litter size in general was ~30-40% smaller, though this observation was based only on a limited number of litters produced. The smaller litter size might reflect potential constrains imposed by the size of the KO dam. Mice born from homozygous KO (-/-) parents appeared largely normal with no gross physical or behavioral abnormalities noted except their pronounced dwarfism. Together, these data indicate that Tmem263 is required for postnatal growth and its absence causes postnatal growth retardation.

Pronounced skeletal dysplasia in Tmem263-null mice

In accordance with postnatal growth failure, adult *Tmem263*-KO mice had much shorter femoral bones compared to WT and heterozygous controls (Fig. 3A-B). Quantification of various bone parameters of distal femur indicated a marked reduction in trabecular bone volume, trabecular number, trabecular bone thickness, cortical tissue area, and cortical thickness in *Tmem263*-KO relative to WT and heterozygous mice (Fig. 3C-H). However, normalization of cortical tissue area and cortical thickness to femur length indicated that skeletal geometry was proportional to that in WT littermates (Fig. 3I-J). Histological analysis revealed a much thinner growth plate in *Tmem263*-KO mice (Fig. 3K). Examination of growth plate morphology in the proximal tibia revealed a reduction in total growth plate length that was secondary to reductions in proliferative zone length in *Tmem263*-KO mice relative to WT controls (Fig. 3L-M). The hypertrophic zone length was not different between genotypes (Fig. 3N). Together, these data indicate that Tmem263 deficiency severely affects postnatal skeletal growth and acquisition.

Tmem263-null mice have low IGF-1, IGFBP3, and IGFALS levels

The GH/IGF-1 axis plays an essential role in postnatal growth and its deficiency results in growth failure (9, 11, 30). The growth retardation and skeletal dysplasia phenotypes seen in *Tmem263*-KO mice strongly suggest a potential deficit in the GH/IGF-1 axis. *Tmem263*-KO mice had a marginal, though not significant, increase in serum GH compared to WT controls (Fig. 4A). However, Serum IGF-1, IGF binding protein 3 (IGFBP3), and IGF acid labile

subunit (IGFALS) levels were markedly lower in *Tmem263*-KO mice relative to WT controls (Fig. 4B-D). Serum insulin levels were significantly lower in KO female mice and trended lower in KO male mice relative to WT controls (Fig. 4E). Random-fed blood glucose levels, however, were significantly lower in *Tmem263*-KO mice (Fig. 4F). The combination of lower insulin and blood glucose levels suggests enhanced insulin sensitivity. These clinical features are also commonly seen in patients with GHR mutations (11). Given the bone phenotype seen in the *Tmem263*-KO mice, we also measured serum Ca^{2+} and phosphate levels. While serum Ca^{2+} levels were reduced in Tmem263-KO mice, serum phosphate levels and the Ca^{2+}/P ratio were not different between genotypes (Fig. 4G-I). Together, these data indicate that low IGF-1, IGFBP3, and IGFALS levels likely contribute to growth retardation and skeletal dysplasia in *Tmem263*-KO mice.

Tmem263-null mice have a marked deficit in hepatic GHR expression and signaling

The GH/IGF-1 axis (Fig. 5A) required for postnatal growth consists of 1) hypothalamic GH releasing hormone (GHRH) which induces pituitary GH release; 2) secreted GH then binds to and activates GHR in the liver, bone, and other peripheral tissues to induce the synthesis and secretion of IGF-1; 3) the direct effects of GH on bone, together with the endocrine and autocrine/paracrine actions of IGF-1, promote longitudinal bone growth (15, 31-33). A majority (~75%) of the circulating IGF-1 is secreted by liver (31). Because *Tmem263*-KO mice had normal to marginally higher GH but low IGF-1 and IGFBP3 levels, the GH/IGF-1 axis is likely disrupted at the liver. Indeed, the expression of *Ghr*, *Igf-1*, and *Igfals* (IGF binding protein acid labile subunit) transcripts was significantly reduced (~4 fold) in the liver of *Tmem263*-KO mice relative to WT controls (Fig. 5B). The expression of *Igfbp3*, however, was not different between genotypes. Consistent with the mRNA data, the hepatic Ghr protein level was similarly and greatly reduced in *Tmem263*-KO mice compared to WT controls (Fig. 5C-D).

Reduced Ghr transcript and protein expression would diminish the magnitude of GH-induced signaling, resulting in GH insensitivity. To test this, mice were injected with recombinant GH and GH-induced signaling in liver was assessed. Janus kinase 2 (JAK2) and Signal transducer and activator of transcription 5b (STAT5b) phosphorylation are the key essential signaling events downstream of the GHR (27, 34). Relative to WT controls, GH injection elicited a greatly diminished response in *Tmem263*-KO mice, as indicated by the much lower magnitude (~60-80% reduction) of Jak2 and Stat5b phosphorylation relative to WT controls (Fig. 5E-F). Together, these data

point to reduced hepatic GHR expression and GH insensitivity as the cause of growth failure and skeletal dysplasia seen in the *Tmem263*-KO animals.

Loss of Tmem263 dramatically affects GH-regulated genes in the liver

Based on our current data and what is known in the literature (35, 36), impaired GH signaling results in widespread changes in the GH-regulated liver transcriptome of *Tmem263*-KO male mice. Indeed, 8.6% of the liver transcriptome in *Tmem263*-KO male mice were significantly altered relative to WT controls, with 1547 protein-coding genes upregulated and 862 protein-coding genes downregulated (Fig. 6A). Among the major classes of genes and pathways most affected by the loss of Tmem263 are those that involved in lipid and steroid metabolism, detoxification process, and xenobiotic handling (Fig. 6B); all of the affected genes and pathways are known to be markedly altered in male mice in which GH signaling is disrupted due to Stat5b deficiency or an altered GH secretory profile (i.e., loss of pulsatile release of GH) (21, 35-40).

It is well known that GH and its distinct secretory profiles (continuous in females vs. intermittent in males) plays a critical role in establishing and maintaining sexually dimorphic gene expression in the liver of male versus female mice (39-43). In male mice, when GH signaling or secretory profile is disrupted, the expression of male-bias genes is dramatically suppressed and, concomitantly, the expression of female-bias genes are upregulated due to their de-repression in male mice (39, 42, 44). This is thought to be the result of altered male-bias (e.g., Foxa1, Bcl6) and female-bias (e.g., Cux2) transcription factor expression that reciprocally regulates the hepatic expression of sex-bias genes in male and female mice (45-47). In male mice with disrupted GH signaling, *Bcl6* expression is suppressed and *Cux2* expression is markedly upregulated, leading to transcriptional repression of male-bias genes and upregulation of female-bias genes in the male liver (39). Remarkably, *Cux2* was one of the most upregulated genes in general and was the most upregulated transcription factor gene in the liver of *Tmem263*-KO male mice (Fig. 6C). The expression of *Bcl6* and *Foxa1*, two male-bias transcription factor genes, were also significantly downregulated in the KO male liver (Fig. 6C). Consequently, all the well-known GH-regulated male-bias genes (growth and metabolism, cytochrome P450, and major urinary protein) were dramatically suppressed due to greatly diminished GH signaling, whereas the female-bias genes (e.g., distinct set of cytochrome P450) were concomitantly and markedly upregulated due to *Cux2* overexpression in the male KO liver (Fig. 6D-F). Together, these

transcriptomic data provide further evidence that the underlying cause of the severe growth retardation and skeletal dysplasia seen in Tmem263-KO mice is indeed attributed, in large part, to disrupted hepatic GH signaling (Fig. 6G).

DISCUSSION

TMEM263 is a GWAS candidate gene associated with BMD (6). In this study, we used a genetic approach to functionally validated its causal role in postnatal growth. Mice lacking Tmem263 showed severe postnatal growth failure and had dramatically reduced bone volume and growth plate length. This phenotype was due to a disrupted GH/IGF-1 axis stemming from hepatic GH insensitivity and low IGF-1 production. This is the first study documenting the physiological function of this enigmatic, but highly conserved, membrane protein.

Since Laron's first description of dwarfism in humans due to defects in the GHR (48-50), an enormous amount of progress has been made to understand how GH and IGF-1, as well as their binding proteins, receptors, and signaling pathways, contribute to linear growth (9, 11, 27, 30). In humans and animal models, defects in any component of the GH/IGF-1 axis leads to a variable severity of postnatal growth failure (short stature) and skeletal dysplasia. These include the initial discoveries of human mutations in GH (51-53), GHR (24, 54-56), IGF-1 (25), IGF-1 receptor (26, 57, 58), STAT5b (20, 59, 60), IGF-1 acid labile subunit (IGFALS) (61, 62), protein tyrosine phosphatase non-receptor type 11 (PTPN11/SHP-2) (63, 64), and pregnancy-associated plasma protein 2A (PAPPA2) (65). The direct causal roles for these genes in regulating growth and skeletal acquisition have also been independently confirmed in genetic mouse models lacking one or more components of the GH/IGF-1 axis (10, 14, 15, 17, 18). Because IGF-1 expression and secretion is directly regulated by GH (66-68), defects in the GH/IGF-1 axis would result in GH insensitivity (GHI), highlighted by the failure of endogenous or exogenously derived GH to elevate plasma IGF-1 levels (9, 11, 30). In the clinical context, the cardinal biochemical features of GHI states are low circulating IGF-1 and normal or increased GH levels (9, 11).

Interestingly, *Tmem263*-KO mice exhibited phenotypes closely resembling *Ghr* and *Igf-1* KO mice (15-17) and humans with GHI. The dwarf *Tmem263*-KO mice had normal to marginally higher serum GH, but low IGF-1,

IGFBP3, and IGFALS levels. The critical proximal signaling events activated by GH binding to the GHR involves JAK2 kinase and the transcription factor STAT5b (27). Failure of STAT5b to bind to the cytoplasmic tails of the GHR due to a truncation mutation also leads to growth failure and a GHI state (69). In *Tmem263*-KO mice, GH injection elicited a greatly muted JAK2/STAT5 signaling response relative to WT controls. This combination of phenotypes, along with marked deficit in bone growth, clearly points to a defect in GHR signaling.

What is the possible cause of GHI seen in *Tmem263*-KO mice? One explanation is the striking reduction in hepatic Ghr protein level induced by the loss of Tmem263. Because we also observed reduced expression of hepatic *Ghr* transcript, the decrease in Ghr protein level reflects, at least in part, lower transcription of the *Ghr* gene. How a deficiency in Tmem263, a putative plasma membrane protein, led to altered hepatic *Ghr* expression and protein level is presently unknown. We cannot, however, exclude the possibility that Tmem263 plays a posttranscriptional role in Ghr processing, stability, turnover, trafficking, and/or signaling. Trafficking defect in GHR has been previously documented, where mutations located at the extracellular domain of the GHR failed to localize to the plasma membrane when expressed in cultured cells (70-72). Whether these mutations affect protein folding and/or a transport signal recognized by another protein has not been established. One important question to address is whether TMEM263 physically interacts with GHR along the secretory pathway or on the plasma membrane of hepatocytes. If such physical association exists, it might provide mechanistic insights into how TMEM263 regulates GHR function. Since both human and mouse *TMEM263* and *GHR* are widely expressed across tissues (73), as well as being most highly expressed in liver, the loss of Tmem263 in the KO mice may have a disproportionate impact on hepatic Ghr function. The generation and characterization of *Tmem263* cell-selective and tissue-specific KOs will help unravel the impact of this protein across different organ systems.

It is not known whether the dwarf chicken with a loss-of-function mutation in *TMEM263* is also insensitive to GH stimulation. To date, there is only one documented case of a loss-of-function mutation in T*MEM263*, and it was associated with severe skeletal dysplasia in a fetus (8). Because pregnancy was terminated before full term, it is unclear whether this mutation is compatible with postnatal survival and its impact on the severity of postnatal growth retardation. Nevertheless, it is tempting to speculate on the possibility that rare homozygous loss-of-function mutations and variants of TMEM264 may cause Laron-type dwarfism with characteristic GHI.

Intriguingly, only one homozygous missense mutation in the *TMEM263* gene has been discovered thus far from over 141,000 aggregated human exomes and genomes sequenced (Genome Aggregation Database; gnomAD v2.1.1) (74). Rare heterozygous splice-site, frameshift, and nonsense mutations in the *TMEM263* gene have also been documented in the gnomAD database (https://gnomad.broadinstitute.org/). Since the Asp-17 residue is highly conserved from fish to man, we speculate that the homozygous D17N missense mutation found in 40 individuals may impact TMEM263 function and affect postnatal linear growth. It would be of considerable interest to ascertain whether individuals with the D17N variant have short stature. Since TMEM263 has not yet been associated with postnatal dwarfism in human, it should be considered a potential candidate gene in screening children with idiopathic growth failure.

MATERIALS AND METHODS

Mouse model

The *Tmem263* knockout (KO) mouse strain was generated at the Johns Hopkins University School of Medicine Transgenic Core facility. To obtain a *Tmem263*-null allele, exon 3 that encodes ~81% of the full-length protein (GenBank # NP_689474) was deleted with the CRISPR/Cas9 method. The deletion encompasses amino acid 23 to 115. The two guide RNAs (gRNA) used were 5'-CTATCATATGTCTCTCATTAG-3' and 5'-GCCACTGGCATCA TATGCTG-3'. The *Tmem263* KO mice were generated and maintained on a C57BL/6J genetic background. Genotyping primers for *Tmem263* wild-type (WT) allele were forward (263-F2) 5'-GCAAGAGCTCCTTACTTAC TCAG-3' and reverse (263-R1) 5'- GATAAGGGCACTTTGTTTACAACTG -3'. The size of the WT band was 391 bp. Genotyping primers for the *Tmem263* KO allele were forward (263-F2) 5'-GCAAGAGCTCCTTACTTACTCA G-3' and reverse (263-R2) 5'-TCACCAATACTTTCAACACAGCAG-3'. The size of the KO band was 218 bp. The GoTaq Green Master Mix (Promega, M7123) was used for PCR genotyping. The genotyping PCR parameters were as follows: 94°C for 5 min, followed by 10 cycles of (94°C for 10 sec, 65°C for 15 sec, 72°C for 30 sec), then 25 cycles of (94°C for 10 sec, 55°C for 15 sec, 72°C for 30 sec), and lastly 72°C for 5 min. Genotyping PCR products from WT and KO mice were excised and confirmed by DNA sequencing. All mice were generated by intercrossing *Tmem263* heterozygous (+/-) mice. *Tmem263* WT (+/+), heterozygous (+/-), and KO (-/-) littermates were housed in polycarbonate cages on a 12-h light–dark photocycle with ad libitum access to water and food. Mice were fed a

standard chow (Envigo; 2018SX). At termination of the study, all mice were fasted for 1-2 h and euthanized. Tissues were collected, snap-frozen in liquid nitrogen, and kept at -80°C until analysis. All mouse protocols (protocol # MO22M367) were approved by the Institutional Animal Care and Use Committee of the Johns Hopkins University School of Medicine. All animal experiments were conducted in accordance with the National Institute of Health guidelines and followed the standards established by the Animal Welfare Acts.

Expression plasmid and antibodies

Mammalian expression plasmid encoding human TMEM263 with a C-terminal epitope tag (Myc-DDK) was obtained from Origene (RC203933). Control pCDNA3.1 empty plasmid was obtained from Invitrogen. Rabbit polyclonal anti-human C12orf23 (TMEM263) was from Origene (TA333490). Mouse monoclonal JAK2 (C-10), STAT5 (A-9), growth hormone receptor (GHR)(B-12) were obtained from Santa Cruz (sc-390539, and sc-74442, and sc-137184, respectively). Rabbit monoclonal antibody against phospho-JAK2 (Tyr1008)(D4A8) were obtained from Cell Signaling Technology (CST # 8082). Rabbit polyclonal antibody against phospho-STAT5 (Y694) was obtained from Cell Signaling Technology (CST#9351). Mouse monoclonal anti-FLAG M2 antibody (F1804) and mouse monoclonal anti-β-actin antibody (A1978) were obtained from Sigma. HRP-conjugated goat anti-rabbit (CST#7074) and goal anti-mouse (CST#7076) antibodies were from Cell Signaling Technology.

Cell surface biotinylation

Cell surface proteins from transfected HEK293 cells were biotinylated using the Pierce Cell Surface Protein Isolation Kit (ThermoFisher Scientific., cat# 89881). Briefly, transfected cells were washed with ice-cold PBS, then incubated with the cell-impermeable biotinylation reagent (Sulfo-NHS-SS-Biotin) for 30 min at 4°C to prevent endocytosis. A quenching solution was then used to stop biotinylation. Cells were collected in a clean tube and centrifuged at 500 *g* for 3 min. The cell pellet was then lysed with RIPA buffer (10 mM Tris-HCl pH 8.0, 1 mM EDTA, 1% Triton X-100, 0.1% Sodium Deoxycholate, 0.1% Sodium Dodecyl Sulfate, 140 mM NaCl, 1 mM PMSF) supplemented with protease inhibitor cocktail (Roche, 11836153001) for 30 min on ice. Cell lysate was then centrifuged at 10,000 *g* for 2 min at 4°C and the resultant supernatant was collected. Biotinylated proteins were pulled-down with Pierce NeutrAvidin Agarose (ThermoFisher Scientific; 29200) at room temperature for 1 h mixed end-over-end. Bound

proteins were eluted from the agarose by DTT (50 mM, final) and heat (94°C for 3 min). Fractions of the input cell lysate, flow-through/non-bound solution, and eluate were used for immunoblot analysis.

Skeletal Phenotyping

For Alcian blue/Alizarin red stained whole mounts, skeletal preps were preformed using P0 neonates following established protocols (75). Briefly, carcasses were macerated by removing skin, eyes, internal organs, and adipose tissue before dehydrating in 95% ethanol overnight and then fixing in acetone. Cartilage was stained by submerging in Alcian blue solution overnight at room temperature. Mineralized tissue was stained by submerging in Alizarin red solution at 4°C overnight.

For microcomputed tomographic analyses of bone structure, high resolution images of the mouse femur were acquired using a desktop microtomographic imaging system (Skyscan 1172, Bruker, Belgium) in accordance with the recommendation of the American Society for Bone and Mineral Research (76). Samples were scanned with an isotropic voxel size of 10μm at 65KeV and 153μA using a 1.0mm aluminum filter. The resulting images were reconstructed using NRecon (Bruker). Trabecular bone parameters in the distal femur of control mice were assessed in a region of interest 500μm proximal to the growth plate and extending for 2mm, while femoral cortical bone parameters were assessed in a 500μm region of interest centered on the mid-diaphysis. Due to the reduced size of the *Tmem263*-KO mice, regions of interest were adjusted to be proportional for tissue length. Trabecular bone parameters were assessed in an ROI 300μm proximal to the growth plate and extending for 1.2mm; cortical bone parameters were assessed in a 300μm ROI centered on the mid-diaphysis.

Growth plate morphology was examined in the proximal tibia. Tibia were dehydrated in graded alcohol solutions and then embedded in methyl methacrylate. 7μm thin sections were cut with a Leica HistoCore Automated Rotary microtome (Leica, Wetzlar, Germany) and stained with Goldner's modified trichrome. Total growth plate length, as well as the lengths of the hypertrophic and proliferative zones were measured with Bioquant Image Analysis software (Bioquant, Nashville, TN).

Western blot analysis

Liver protein was isolated using RIPA buffer as previously described (77). Liver protein lysates used for immunoblots were boiled for 5 min in a loading buffer (50 mM Tris, 2% SDS, 1% β-ME, 6% glycerol, 0.01%

bromophenol blue). Total protein was quantified by BCA assay (Thermo Scientific, 23225), loaded in equal amounts and volume, and run on a 7.5% or 10% TGX gel (Bio-Rad, 4561023 and 4561033). Protein was transferred to PVDF membrane (Bio-Rad, 1620177) using the Trans Blot Turbo system (Bio-Rad) and blocked in PBS containing 0.2% Tween 20 and 5% non-fat milk for 1 h, then incubated overnight at 4°C on a shaker with primary antibody. The following primary antibodies were used: anti-TMEM263 (1:1000), anti-GH-R (1:100), anti-phospho-JAK2 (Tyr1008) (1:500), anti-phospho-STAT5 (Y694) (1:500), anti-JAK2 (1:100), anti-JAK5 (1:100), anti-β-actin (1:2000). Blots were washed at least 3 times (5 min each) with PBS containing 0.2% Tween 20 before secondary antibody was added. HRP-conjugated anti-rabbit or anti-mouse secondary antibody (1:500 to 1:1000; 1 hr at room temperature) were used to recognize the primary antibody. Blots were washed at least 3 times (5 min each) with PBS containing 0.2% Tween 20. Immunoblots were developed using HRP substrate ECL (GE Healthcare), visualized with a MultiImage III FluorChem Q (Alpha Innotech), and quantified with ImageJ (78).

Growth hormone (GH) injection

Recombinant human GH from Peprotech (Cat # 100-40; Cranbury, NJ) was reconstituted in PBS at a concentration 0.2 μg/μL. Each mouse received GH injection at a dose of 3 μg/g body weight. Mice were sacrificed 25 min post GH injection, and the liver was immediately harvested and snap frozen in liquid nitrogen.

Blood and tissue chemistry analysis

Tail vein blood samples were allowed to clot on ice and then centrifuged for 10 min at 10,000 x *g*. Serum samples were stored at -80°C until analyzed. Serum insulin (Crystal Chem, Elk Grove Village, IL; 90080), GH (Millipore Sigma; EZRMGH-45K, Burlington, MA), IGF-1 (Crystal Chem, 80574), IGFBP3 (Abcam; ab100692, Waltham, MA), and IGFALS (Cusabio; CSB-EL011094MO, Houston, TX) levels were measured by ELISA according to manufacturer's instructions. Serum calcium and phosphate levels were quantified at the Molecular and Comparative Pathobiology Core at The Johns Hopkins University School of Medicine using the Respons®910VET Veterinary Chemistry Analyzer (DiaSys Diagnostic Systems, Wixom, MI, USA).

Quantitative real-time PCR analysis

Total RNA was isolated from tissues using Trizol reagent (Thermo Fisher Scientific) according to the manufacturer's instructions. Purified RNA was reverse transcribed using an iScript cDNA Synthesis Kit (Bio-rad). Real-time quantitative PCR analysis was performed on a CFX Connect Real-Time System (Bio-rad) using iTaq™ Universal SYBR Green Supermix (Bio-rad) per manufacturer's instructions. Data were normalized to either *β-actin* or *36B4* gene (encoding the acidic ribosomal phosphoprotein P0) and expressed as relative mRNA levels using the ΔΔCt method (79). Fold change data were log transformed to ensure normal distribution and statistics were performed. Real-time qPCR primers used were: mouse *Tmem263* forward (qPCR-263-F1), 5'-CGCGGTGATCATGAATCAGG CAG-3' and reverse (qPCR-263-R1), 5'-GCTCCCTTTGTAACACTGAAGA-3'; growth hormone receptor (*Ghr*) forward, 5'-ACAGTGCCTACTTTTGTGAGTC-3' and reverse, 5'-GTAGTGGTAAGGCTTTCTGTGG-3'; *Igf-1* forward, 5'-GTGAGCCAAAGACACACCCA-3' and reverse, 5'-ACCTCTGATTTTCCGAGTTGC-3'; *Igfbp3* forward, 5'-CCAGGAAACATCAGTGAG TCC-3' and reverse, 5'-GGATGGAACTTGGAATCGGTCA-3'; *Igfals* forward, 5'-CTGCCCGATAGCATCCCAG-3' and reverse, 5'-GAAGCCAGACTTGGTGTGTGT-3'; *36B4* forward, 5'-AGATTCGGGATATGCTGTTGGC-3' and reverse, 5'-TCGGGTCCTAGACCAGTGTTC-3'; β-actin forward, 5'-GGCACCACACCTTCTACAATG -3' and reverse, 5'-GGGGTGTTGAAGGTCTCAAAC -3'.

RNA-seq and bioinformatics analysis

Bulk RNA sequencing of WT (n = 8) and *Tmem263*-KO (n = 8) mouse liver were performed by Novogene (Sacramento, California, USA) on an Illumina platform (NovaSeq 6000) and pair-end reads were generated. Sequencing data was analyzed using the Novogene Analysis Pipeline. In brief, data analysis was performed using a combination of programs, including Fastp, Hisat2, and FeatureCounts. Differential expressions were determined through DESeq2. The resulting P-values were adjusted using the Benjamini and Hochberg's approach for controlling the false discovery rate. Genes with an adjusted P-value ≤ 0.05 found by DESeq2 were assigned as differentially expressed. Gene ontology (GO), Kyoto Encyclopedia of Genes and Genomes (KEGG), and Reactome (http://www.reactome.org) enrichment were implemented by ClusterProfiler. All volcano plots and heat maps were generated in Graphpad Prism 9 software. All statistics were performed on Log transformed data. All heat maps were generated from column z-score transformed data. The z-score of each column was determined by taking the column average, subtracting each sample's individual expression value by said average then dividing that difference by the column standard deviation. Z-score = (value – column average)/column standard deviation. High-throughput

sequencing data from this study have been submitted to the NCBI Sequence Read Archive (SRA) under accession number # PRJNA938158.

Statistical analyses

All results are expressed as mean ± standard error of the mean (SEM). Statistical analysis was performed with Graphpad Prism 9 software (GraphPad Software, San Diego, CA). Data were analyzed with two-tailed Student's *t*-tests or by one-way ANOVA with Tukey's multiple comparisons test. $P < 0.05$ was considered statistically significant.

ACKNOWLEDGEMENTS

This work was supported by the National Institutes of Health (DK084171 to GWW; AR077533 and DK099134 to RCR). We thank Thomas Clemens for helpful discussion.

COMPETING INTERESTS

We declare that none of the authors has a conflict of interest.

REFERENCES

1. Estrada, K., Styrkarsdottir, U., Evangelou, E., Hsu, Y. H., Duncan, E. L., Ntzani, E. E., Oei, L., Albagha, O. M., Amin, N., Kemp, J. P., Koller, D. L., Li, G., Liu, C. T., Minster, R. L., Moayyeri, A., Vandenput, L., Willner, D., Xiao, S. M., Yerges-Armstrong, L. M., Zheng, H. F., Alonso, N., Eriksson, J., Kammerer, C. M., Kaptoge, S. K., Leo, P. J., Thorleifsson, G., Wilson, S. G., Wilson, J. F., Aalto, V., Alen, M., Aragaki, A. K., Aspelund, T., Center, J. R., Dailiana, Z., Duggan, D. J., Garcia, M., Garcia-Giralt, N., Giroux, S., Hallmans, G., Hocking, L. J., Husted, L. B., Jameson, K. A., Khusainova, R., Kim, G. S., Kooperberg, C., Koromila, T., Kruk, M., Laaksonen, M., Lacroix, A. Z., Lee, S. H., Leung, P. C., Lewis, J. R., Masi, L., Mencej-Bedrac, S., Nguyen, T. V., Nogues, X., Patel, M. S., Prezelj, J., Rose, L. M., Scollen, S., Siggeirsdottir, K., Smith, A. V., Svensson, O., Trompet, S., Trummer, O., van Schoor, N. M., Woo, J., Zhu, K., Balcells, S., Brandi, M. L., Buckley, B. M., Cheng, S., Christiansen, C., Cooper, C., Dedoussis, G., Ford, I., Frost, M., Goltzman, D., Gonzalez-Macias, J., Kahonen, M., Karlsson, M., Khusnutdinova, E., Koh, J. M., Kollia, P., Langdahl, B. L., Leslie, W. D., Lips, P., Ljunggren, O., Lorenc, R. S., Marc, J., Mellstrom, D., Obermayer-Pietsch, B., Olmos, J. M., Pettersson-Kymmer, U., Reid, D. M., Riancho, J. A., Ridker, P. M., Rousseau, F., Slagboom, P. E., Tang, N. L., Urreizti, R., Van Hul, W., Viikari, J., Zarrabeitia, M. T., Aulchenko, Y. S., Castano-Betancourt, M., Grundberg, E., Herrera, L., Ingvarsson, T., Johannsdottir, H., Kwan, T., Li, R., Luben, R., Medina-Gomez, C., Palsson, S. T., Reppe, S., Rotter, J. I., Sigurdsson, G., van Meurs, J. B., Verlaan, D., Williams, F. M., Wood, A. R., Zhou, Y., Gautvik, K. M., Pastinen, T., Raychaudhuri, S., Cauley, J. A., Chasman, D. I., Clark, G. R., Cummings, S. R., Danoy, P., Dennison, E. M., Eastell, R., Eisman, J. A., Gudnason, V., Hofman, A., Jackson, R. D., Jones, G., Jukema, J. W., Khaw, K. T., Lehtimaki, T., Liu, Y., Lorentzon, M., McCloskey, E., Mitchell, B. D., Nandakumar, K., Nicholson, G. C., Oostra, B. A., Peacock, M., Pols, H. A., Prince, R. L., Raitakari, O., Reid, I. R.,

Robbins, J., Sambrook, P. N., Sham, P. C., Shuldiner, A. R., Tylavsky, F. A., van Duijn, C. M., Wareham, N. J., Cupples, L. A., Econs, M. J., Evans, D. M., Harris, T. B., Kung, A. W., Psaty, B. M., Reeve, J., Spector, T. D., Streeten, E. A., Zillikens, M. C., Thorsteinsdottir, U., Ohlsson, C., Karasik, D., Richards, J. B., Brown, M. A., Stefansson, K., Uitterlinden, A. G., Ralston, S. H., Ioannidis, J. P., Kiel, D. P., and Rivadeneira, F. (2012) Genome-wide meta-analysis identifies 56 bone mineral density loci and reveals 14 loci associated with risk of fracture. *Nat Genet* **44**, 491-501

2. Kemp, J. P., Morris, J. A., Medina-Gomez, C., Forgetta, V., Warrington, N. M., Youlten, S. E., Zheng, J., Gregson, C. L., Grundberg, E., Trajanoska, K., Logan, J. G., Pollard, A. S., Sparkes, P. C., Ghirardello, E. J., Allen, R., Leitch, V. D., Butterfield, N. C., Komla-Ebri, D., Adoum, A. T., Curry, K. F., White, J. K., Kussy, F., Greenlaw, K. M., Xu, C., Harvey, N. C., Cooper, C., Adams, D. J., Greenwood, C. M. T., Maurano, M. T., Kaptoge, S., Rivadeneira, F., Tobias, J. H., Croucher, P. I., Ackert-Bicknell, C. L., Bassett, J. H. D., Williams, G. R., Richards, J. B., and Evans, D. M. (2017) Identification of 153 new loci associated with heel bone mineral density and functional involvement of GPC6 in osteoporosis. *Nat Genet* **49**, 1468-1475
3. Zhao, L. J., Liu, X. G., Liu, Y. Z., Liu, Y. J., Papasian, C. J., Sha, B. Y., Pan, F., Guo, Y. F., Wang, L., Yan, H., Xiong, D. H., Tang, Z. H., Yang, T. L., Chen, X. D., Guo, Y., Li, J., Shen, H., Zhang, F., Lei, S. F., Recker, R. R., and Deng, H. W. (2010) Genome-wide association study for femoral neck bone geometry. *J Bone Miner Res* **25**, 320-329
4. Styrkarsdottir, U., Stefansson, O. A., Gunnarsdottir, K., Thorleifsson, G., Lund, S. H., Stefansdottir, L., Juliusson, K., Agustsdottir, A. B., Zink, F., Halldorsson, G. H., Ivarsdottir, E. V., Benonisdottir, S., Jonsson, H., Gylfason, A., Norland, K., Trajanoska, K., Boer, C. G., Southam, L., Leung, J. C. S., Tang, N. L. S., Kwok, T. C. Y., Lee, J. S. W., Ho, S. C., Byrjalsen, I., Center, J. R., Lee, S. H., Koh, J. M., Lohmander, L. S., Ho-Pham, L. T., Nguyen, T. V., Eisman, J. A., Woo, J., Leung, P. C., Loughlin, J., Zeggini, E., Christiansen, C., Rivadeneira, F., van Meurs, J., Uitterlinden, A. G., Mogensen, B., Jonsson, H., Ingvarsson, T., Sigurdsson, G., Benediktsson, R., Sulem, P., Jonsdottir, I., Masson, G., Holm, H., Norddahl, G. L., Thorsteinsdottir, U., Gudbjartsson, D. F., and Stefansson, K. (2019) GWAS of bone size yields twelve loci that also affect height, BMD, osteoarthritis or fractures. *Nature communications* **10**, 2054
5. Chan, Y., Salem, R. M., Hsu, Y. H., McMahon, G., Pers, T. H., Vedantam, S., Esko, T., Guo, M. H., Lim, E. T., Consortium, G., Franke, L., Smith, G. D., Strachan, D. P., and Hirschhorn, J. N. (2015) Genome-wide analysis of body proportion classifies height-associated variants by mechanism of action and implicates genes important for skeletal development. *Am J Hum Genet* **96**, 695-708
6. Calabrese, G. M., Mesner, L. D., Stains, J. P., Tommasini, S. M., Horowitz, M. C., Rosen, C. J., and Farber, C. R. (2017) Integrating GWAS and Co-expression Network Data Identifies Bone Mineral Density Genes SPTBN1 and MARK3 and an Osteoblast Functional Module. *Cell Syst* **4**, 46-59 e44
7. Wu, Z., Derks, M. F. L., Dibbits, B., Megens, H. J., Groenen, M. A. M., and Crooijmans, R. (2018) A Novel Loss-of-Function Variant in Transmembrane Protein 263 (TMEM263) of Autosomal Dwarfism in Chicken. *Front Genet* **9**, 193
8. Mohajeri, M. S. A., Eslahi, A., Khazaii, Z., Moradi, M. R., Pazhoomand, R., Farrokhi, S., Feizabadi, M. H., Alizadeh, F., and Mojarrad, M. (2021) TMEM263: a novel candidate gene implicated in human autosomal recessive severe lethal skeletal dysplasia. *Hum Genomics* **15**, 42
9. David, A., Hwa, V., Metherell, L. A., Netchine, I., Camacho-Hubner, C., Clark, A. J., Rosenfeld, R. G., and Savage, M. O. (2011) Evidence for a continuum of genetic, phenotypic, and biochemical abnormalities in children with growth hormone insensitivity. *Endocr Rev* **32**, 472-497
10. Efstratiadis, A. (1998) Genetics of mouse growth. *Int J Dev Biol* **42**, 955-976
11. Savage, M. O., Hwa, V., David, A., Rosenfeld, R. G., and Metherell, L. A. (2011) Genetic Defects in the Growth Hormone-IGF-I Axis Causing Growth Hormone Insensitivity and Impaired Linear Growth. *Front Endocrinol (Lausanne)* **2**, 95
12. Rosenfeld, R. G., Belgorosky, A., Camacho-Hubner, C., Savage, M. O., Wit, J. M., and Hwa, V. (2007) Defects in growth hormone receptor signaling. *Trends Endocrinol Metab* **18**, 134-141
13. Rosenfeld, R. G., Rosenbloom, A. L., and Guevara-Aguirre, J. (1994) Growth hormone (GH) insensitivity due to primary GH receptor deficiency. *Endocr Rev* **15**, 369-390
14. Qian, Y., Berryman, D. E., Basu, R., List, E. O., Okada, S., Young, J. A., Jensen, E. A., Bell, S. R. C., Kulkarni, P., Duran-Ortiz, S., Mora-Criollo, P., Mathes, S. C., Brittain, A. L., Buchman, M., Davis, E., Funk, K. R., Bogart, J., Ibarra, D., Mendez-Gibson, I., Slyby, J., Terry, J., and Kopchick, J. J. (2022) Mice with gene alterations in the GH and IGF family. *Pituitary* **25**, 1-51

15. Lupu, F., Terwilliger, J. D., Lee, K., Segre, G. V., and Efstratiadis, A. (2001) Roles of growth hormone and insulin-like growth factor 1 in mouse postnatal growth. *Dev Biol* **229**, 141-162
16. Zhou, Y., Xu, B. C., Maheshwari, H. G., He, L., Reed, M., Lozykowski, M., Okada, S., Cataldo, L., Coschigamo, K., Wagner, T. E., Baumann, G., and Kopchick, J. J. (1997) A mammalian model for Laron syndrome produced by targeted disruption of the mouse growth hormone receptor/binding protein gene (the Laron mouse). *Proc Natl Acad Sci U S A* **94**, 13215-13220
17. Baker, J., Liu, J. P., Robertson, E. J., and Efstratiadis, A. (1993) Role of insulin-like growth factors in embryonic and postnatal growth. *Cell* **75**, 73-82
18. Liu, J. P., Baker, J., Perkins, A. S., Robertson, E. J., and Efstratiadis, A. (1993) Mice carrying null mutations of the genes encoding insulin-like growth factor I (Igf-1) and type 1 IGF receptor (Igf1r). *Cell* **75**, 59-72
19. Davey, H. W., Wilkins, R. J., and Waxman, D. J. (1999) STAT5 signaling in sexually dimorphic gene expression and growth patterns. *Am J Hum Genet* **65**, 959-965
20. Kofoed, E. M., Hwa, V., Little, B., Woods, K. A., Buckway, C. K., Tsubaki, J., Pratt, K. L., Bezrodnik, L., Jasper, H., Tepper, A., Heinrich, J. J., and Rosenfeld, R. G. (2003) Growth hormone insensitivity associated with a STAT5b mutation. *N Engl J Med* **349**, 1139-1147
21. Udy, G. B., Towers, R. P., Snell, R. G., Wilkins, R. J., Park, S. H., Ram, P. A., Waxman, D. J., and Davey, H. W. (1997) Requirement of STAT5b for sexual dimorphism of body growth rates and liver gene expression. *Proc Natl Acad Sci U S A* **94**, 7239-7244
22. Hwa, V., Camacho-Hubner, C., Little, B. M., David, A., Metherell, L. A., El-Khatib, N., Savage, M. O., and Rosenfeld, R. G. (2007) Growth hormone insensitivity and severe short stature in siblings: a novel mutation at the exon 13-intron 13 junction of the STAT5b gene. *Horm Res* **68**, 218-224
23. Klammt, J., Neumann, D., Gevers, E. F., Andrew, S. F., Schwartz, I. D., Rockstroh, D., Colombo, R., Sanchez, M. A., Vokurkova, D., Kowalczyk, J., Metherell, L. A., Rosenfeld, R. G., Pfaffle, R., Dattani, M. T., Dauber, A., and Hwa, V. (2018) Dominant-negative STAT5B mutations cause growth hormone insensitivity with short stature and mild immune dysregulation. *Nature communications* **9**, 2105
24. Godowski, P. J., Leung, D. W., Meacham, L. R., Galgani, J. P., Hellmiss, R., Keret, R., Rotwein, P. S., Parks, J. S., Laron, Z., and Wood, W. I. (1989) Characterization of the human growth hormone receptor gene and demonstration of a partial gene deletion in two patients with Laron-type dwarfism. *Proc Natl Acad Sci U S A* **86**, 8083-8087
25. Woods, K. A., Camacho-Hubner, C., Savage, M. O., and Clark, A. J. (1996) Intrauterine growth retardation and postnatal growth failure associated with deletion of the insulin-like growth factor I gene. *N Engl J Med* **335**, 1363-1367
26. Abuzzahab, M. J., Schneider, A., Goddard, A., Grigorescu, F., Lautier, C., Keller, E., Kiess, W., Klammt, J., Kratzsch, J., Osgood, D., Pfaffle, R., Raile, K., Seidel, B., Smith, R. J., Chernausek, S. D., and Intrauterine Growth Retardation Study, G. (2003) IGF-I receptor mutations resulting in intrauterine and postnatal growth retardation. *N Engl J Med* **349**, 2211-2222
27. Lanning, N. J., and Carter-Su, C. (2006) Recent advances in growth hormone signaling. *Rev Endocr Metab Disord* **7**, 225-235
28. Uhlen, M., Fagerberg, L., Hallstrom, B. M., Lindskog, C., Oksvold, P., Mardinoglu, A., Sivertsson, A., Kampf, C., Sjostedt, E., Asplund, A., Olsson, I., Edlund, K., Lundberg, E., Navani, S., Szigyarto, C. A., Odeberg, J., Djureinovic, D., Takanen, J. O., Hober, S., Alm, T., Edqvist, P. H., Berling, H., Tegel, H., Mulder, J., Rockberg, J., Nilsson, P., Schwenk, J. M., Hamsten, M., von Feilitzen, K., Forsberg, M., Persson, L., Johansson, F., Zwahlen, M., von Heijne, G., Nielsen, J., and Ponten, F. (2015) Proteomics. Tissue-based map of the human proteome. *Science* **347**, 1260419
29. Consortium, G. T. (2015) Human genomics. The Genotype-Tissue Expression (GTEx) pilot analysis: multitissue gene regulation in humans. *Science* **348**, 648-660
30. Hwa, V., Fujimoto, M., Zhu, G., Gao, W., Foley, C., Kumbaji, M., and Rosenfeld, R. G. (2021) Genetic causes of growth hormone insensitivity beyond GHR. *Rev Endocr Metab Disord* **22**, 43-58
31. Ohlsson, C., Mohan, S., Sjogren, K., Tivesten, A., Isgaard, J., Isaksson, O., Jansson, J. O., and Svensson, J. (2009) The role of liver-derived insulin-like growth factor-I. *Endocr Rev* **30**, 494-535
32. Stratikopoulos, E., Szabolcs, M., Dragatsis, I., Klinakis, A., and Efstratiadis, A. (2008) The hormonal action of IGF1 in postnatal mouse growth. *Proc Natl Acad Sci U S A* **105**, 19378-19383
33. Wu, Y., Sun, H., Yakar, S., and LeRoith, D. (2009) Elevated levels of insulin-like growth factor (IGF)-I in serum rescue the severe growth retardation of IGF-I null mice. *Endocrinology* **150**, 4395-4403

34. Rosenfeld, R. G., and Hwa, V. (2009) The growth hormone cascade and its role in mammalian growth. *Horm Res* **71 Suppl 2**, 36-40
35. Clodfelter, K. H., Holloway, M. G., Hodor, P., Park, S. H., Ray, W. J., and Waxman, D. J. (2006) Sex-dependent liver gene expression is extensive and largely dependent upon signal transducer and activator of transcription 5b (STAT5b): STAT5b-dependent activation of male genes and repression of female genes revealed by microarray analysis. *Mol Endocrinol* **20**, 1333-1351
36. Holloway, M. G., Cui, Y., Laz, E. V., Hosui, A., Hennighausen, L., and Waxman, D. J. (2007) Loss of sexually dimorphic liver gene expression upon hepatocyte-specific deletion of Stat5a-Stat5b locus. *Endocrinology* **148**, 1977-1986
37. Davey, H. W., Park, S. H., Grattan, D. R., McLachlan, M. J., and Waxman, D. J. (1999) STAT5b-deficient mice are growth hormone pulse-resistant. Role of STAT5b in sex-specific liver p450 expression. *J Biol Chem* **274**, 35331-35336
38. Holloway, M. G., Laz, E. V., and Waxman, D. J. (2006) Codependence of growth hormone-responsive, sexually dimorphic hepatic gene expression on signal transducer and activator of transcription 5b and hepatic nuclear factor 4alpha. *Mol Endocrinol* **20**, 647-660
39. Lau-Corona, D., Suvorov, A., and Waxman, D. J. (2017) Feminization of Male Mouse Liver by Persistent Growth Hormone Stimulation: Activation of Sex-Biased Transcriptional Networks and Dynamic Changes in Chromatin States. *Mol Cell Biol* **37**
40. Waxman, D. J., Pampori, N. A., Ram, P. A., Agrawal, A. K., and Shapiro, B. H. (1991) Interpulse interval in circulating growth hormone patterns regulates sexually dimorphic expression of hepatic cytochrome P450. *Proc Natl Acad Sci U S A* **88**, 6868-6872
41. Zhang, Y., Laz, E. V., and Waxman, D. J. (2012) Dynamic, sex-differential STAT5 and BCL6 binding to sex-biased, growth hormone-regulated genes in adult mouse liver. *Mol Cell Biol* **32**, 880-896
42. Waxman, D. J., and O'Connor, C. (2006) Growth hormone regulation of sex-dependent liver gene expression. *Mol Endocrinol* **20**, 2613-2629
43. Norstedt, G., and Palmiter, R. (1984) Secretory rhythm of growth hormone regulates sexual differentiation of mouse liver. *Cell* **36**, 805-812
44. Chia, D. J. (2014) Minireview: mechanisms of growth hormone-mediated gene regulation. *Mol Endocrinol* **28**, 1012-1025
45. Conforto, T. L., Zhang, Y., Sherman, J., and Waxman, D. J. (2012) Impact of CUX2 on the female mouse liver transcriptome: activation of female-biased genes and repression of male-biased genes. *Mol Cell Biol* **32**, 4611-4627
46. Sugathan, A., and Waxman, D. J. (2013) Genome-wide analysis of chromatin states reveals distinct mechanisms of sex-dependent gene regulation in male and female mouse liver. *Mol Cell Biol* **33**, 3594-3610
47. Meyer, R. D., Laz, E. V., Su, T., and Waxman, D. J. (2009) Male-specific hepatic Bcl6: growth hormone-induced block of transcription elongation in females and binding to target genes inversely coordinated with STAT5. *Mol Endocrinol* **23**, 1914-1926
48. Eshet, R., Laron, Z., Pertzelan, A., Arnon, R., and Dintzman, M. (1984) Defect of human growth hormone receptors in the liver of two patients with Laron-type dwarfism. *Isr J Med Sci* **20**, 8-11
49. Laron, Z. (2004) Laron syndrome (primary growth hormone resistance or insensitivity): the personal experience 1958-2003. *J Clin Endocrinol Metab* **89**, 1031-1044
50. Laron, Z., Pertzelan, A., and Mannheimer, S. (1966) Genetic pituitary dwarfism with high serum concentation of growth hormone--a new inborn error of metabolism? *Isr J Med Sci* **2**, 152-155
51. Takahashi, Y., Kaji, H., Okimura, Y., Goji, K., Abe, H., and Chihara, K. (1996) Brief report: short stature caused by a mutant growth hormone. *N Engl J Med* **334**, 432-436
52. Takahashi, Y., Shirono, H., Arisaka, O., Takahashi, K., Yagi, T., Koga, J., Kaji, H., Okimura, Y., Abe, H., Tanaka, T., and Chihara, K. (1997) Biologically inactive growth hormone caused by an amino acid substitution. *J Clin Invest* **100**, 1159-1165
53. Besson, A., Salemi, S., Deladoey, J., Vuissoz, J. M., Eble, A., Bidlingmaier, M., Burgi, S., Honegger, U., Fluck, C., and Mullis, P. E. (2005) Short stature caused by a biologically inactive mutant growth hormone (GH-C53S). *J Clin Endocrinol Metab* **90**, 2493-2499
54. Amselem, S., Duquesnoy, P., Attree, O., Novelli, G., Bousnina, S., Postel-Vinay, M. C., and Goossens, M. (1989) Laron dwarfism and mutations of the growth hormone-receptor gene. *N Engl J Med* **321**, 989-995

55. Amselem, S., Sobrier, M. L., Duquesnoy, P., Rappaport, R., Postel-Vinay, M. C., Gourmelen, M., Dallapiccola, B., and Goossens, M. (1991) Recurrent nonsense mutations in the growth hormone receptor from patients with Laron dwarfism. *J Clin Invest* **87**, 1098-1102
56. Berg, M. A., Argente, J., Chernausek, S., Gracia, R., Guevara-Aguirre, J., Hopp, M., Perez-Jurado, L., Rosenbloom, A., Toledo, S. P., and Francke, U. (1993) Diverse growth hormone receptor gene mutations in Laron syndrome. *Am J Hum Genet* **52**, 998-1005
57. Kawashima, Y., Kanzaki, S., Yang, F., Kinoshita, T., Hanaki, K., Nagaishi, J., Ohtsuka, Y., Hisatome, I., Ninomoya, H., Nanba, E., Fukushima, T., and Takahashi, S. (2005) Mutation at cleavage site of insulin-like growth factor receptor in a short-stature child born with intrauterine growth retardation. *J Clin Endocrinol Metab* **90**, 4679-4687
58. Inagaki, K., Tiulpakov, A., Rubtsov, P., Sverdlova, P., Peterkova, V., Yakar, S., Terekhov, S., and LeRoith, D. (2007) A familial insulin-like growth factor-I receptor mutant leads to short stature: clinical and biochemical characterization. *J Clin Endocrinol Metab* **92**, 1542-1548
59. Hwa, V., Little, B., Adiyaman, P., Kofoed, E. M., Pratt, K. L., Ocal, G., Berberoglu, M., and Rosenfeld, R. G. (2005) Severe growth hormone insensitivity resulting from total absence of signal transducer and activator of transcription 5b. *J Clin Endocrinol Metab* **90**, 4260-4266
60. Vidarsdottir, S., Walenkamp, M. J., Pereira, A. M., Karperien, M., van Doorn, J., van Duyvenvoorde, H. A., White, S., Breuning, M. H., Roelfsema, F., Kruithof, M. F., van Dissel, J., Janssen, R., Wit, J. M., and Romijn, J. A. (2006) Clinical and biochemical characteristics of a male patient with a novel homozygous STAT5b mutation. *J Clin Endocrinol Metab* **91**, 3482-3485
61. Domene, H. M., Bengolea, S. V., Martinez, A. S., Ropelato, M. G., Pennisi, P., Scaglia, P., Heinrich, J. J., and Jasper, H. G. (2004) Deficiency of the circulating insulin-like growth factor system associated with inactivation of the acid-labile subunit gene. *N Engl J Med* **350**, 570-577
62. Domene, H. M., Scaglia, P. A., Lteif, A., Mahmud, F. H., Kirmani, S., Frystyk, J., Bedecarras, P., Gutierrez, M., and Jasper, H. G. (2007) Phenotypic effects of null and haploinsufficiency of acid-labile subunit in a family with two novel IGFALS gene mutations. *J Clin Endocrinol Metab* **92**, 4444-4450
63. Tartaglia, M., Mehler, E. L., Goldberg, R., Zampino, G., Brunner, H. G., Kremer, H., van der Burgt, I., Crosby, A. H., Ion, A., Jeffery, S., Kalidas, K., Patton, M. A., Kucherlapati, R. S., and Gelb, B. D. (2001) Mutations in PTPN11, encoding the protein tyrosine phosphatase SHP-2, cause Noonan syndrome. *Nat Genet* **29**, 465-468
64. Binder, G., Neuer, K., Ranke, M. B., and Wittekindt, N. E. (2005) PTPN11 mutations are associated with mild growth hormone resistance in individuals with Noonan syndrome. *J Clin Endocrinol Metab* **90**, 5377-5381
65. Dauber, A., Munoz-Calvo, M. T., Barrios, V., Domene, H. M., Kloverpris, S., Serra-Juhe, C., Desikan, V., Pozo, J., Muzumdar, R., Martos-Moreno, G. A., Hawkins, F., Jasper, H. G., Conover, C. A., Frystyk, J., Yakar, S., Hwa, V., Chowen, J. A., Oxvig, C., Rosenfeld, R. G., Perez-Jurado, L. A., and Argente, J. (2016) Mutations in pregnancy-associated plasma protein A2 cause short stature due to low IGF-I availability. *EMBO Mol Med* **8**, 363-374
66. Chia, D. J., Varco-Merth, B., and Rotwein, P. (2010) Dispersed Chromosomal Stat5b-binding elements mediate growth hormone-activated insulin-like growth factor-I gene transcription. *J Biol Chem* **285**, 17636-17647
67. Woelfle, J., Billiard, J., and Rotwein, P. (2003) Acute control of insulin-like growth factor-I gene transcription by growth hormone through Stat5b. *J Biol Chem* **278**, 22696-22702
68. Woelfle, J., Chia, D. J., and Rotwein, P. (2003) Mechanisms of growth hormone (GH) action. Identification of conserved Stat5 binding sites that mediate GH-induced insulin-like growth factor-I gene activation. *J Biol Chem* **278**, 51261-51266
69. Milward, A., Metherell, L., Maamra, M., Barahona, M. J., Wilkinson, I. R., Camacho-Hubner, C., Savage, M. O., Bidlingmaier, M., Clark, A. J., Ross, R. J., and Webb, S. M. (2004) Growth hormone (GH) insensitivity syndrome due to a GH receptor truncated after Box1, resulting in isolated failure of STAT 5 signal transduction. *J Clin Endocrinol Metab* **89**, 1259-1266
70. Duquesnoy, P., Sobrier, M. L., Amselem, S., and Goossens, M. (1991) Defective membrane expression of human growth hormone (GH) receptor causes Laron-type GH insensitivity syndrome. *Proc Natl Acad Sci U S A* **88**, 10272-10276

71. Maamra, M., Milward, A., Esfahani, H. Z., Abbott, L. P., Metherell, L. A., Savage, M. O., Clark, A. J., and Ross, R. J. (2006) A 36 residues insertion in the dimerization domain of the growth hormone receptor results in defective trafficking rather than impaired signaling. *J Endocrinol* **188**, 251-261
72. Fang, P., Girgis, R., Little, B. M., Pratt, K. L., Guevara-Aguirre, J., Hwa, V., and Rosenfeld, R. G. (2008) Growth hormone (GH) insensitivity and insulin-like growth factor-I deficiency in Inuit subjects and an Ecuadorian cohort: functional studies of two codon 180 GH receptor gene mutations. *J Clin Endocrinol Metab* **93**, 1030-1037
73. Ballesteros, M., Leung, K. C., Ross, R. J., Iismaa, T. P., and Ho, K. K. (2000) Distribution and abundance of messenger ribonucleic acid for growth hormone receptor isoforms in human tissues. *J Clin Endocrinol Metab* **85**, 2865-2871
74. Karczewski, K. J., Francioli, L. C., Tiao, G., Cummings, B. B., Alfoldi, J., Wang, Q., Collins, R. L., Laricchia, K. M., Ganna, A., Birnbaum, D. P., Gauthier, L. D., Brand, H., Solomonson, M., Watts, N. A., Rhodes, D., Singer-Berk, M., England, E. M., Seaby, E. G., Kosmicki, J. A., Walters, R. K., Tashman, K., Farjoun, Y., Banks, E., Poterba, T., Wang, A., Seed, C., Whiffin, N., Chong, J. X., Samocha, K. E., Pierce-Hoffman, E., Zappala, Z., O'Donnell-Luria, A. H., Minikel, E. V., Weisburd, B., Lek, M., Ware, J. S., Vittal, C., Armean, I. M., Bergelson, L., Cibulskis, K., Connolly, K. M., Covarrubias, M., Donnelly, S., Ferriera, S., Gabriel, S., Gentry, J., Gupta, N., Jeandet, T., Kaplan, D., Llanwarne, C., Munshi, R., Novod, S., Petrillo, N., Roazen, D., Ruano-Rubio, V., Saltzman, A., Schleicher, M., Soto, J., Tibbetts, K., Tolonen, C., Wade, G., Talkowski, M. E., Genome Aggregation Database, C., Neale, B. M., Daly, M. J., and MacArthur, D. G. (2020) The mutational constraint spectrum quantified from variation in 141,456 humans. *Nature* **581**, 434-443
75. Rigueur, D., and Lyons, K. M. (2014) Whole-mount skeletal staining. *Methods Mol Biol* **1130**, 113-121
76. Bouxsein, M. L., Boyd, S. K., Christiansen, B. A., Guldberg, R. E., Jepsen, K. J., and Muller, R. (2010) Guidelines for assessment of bone microstructure in rodents using micro-computed tomography. *J Bone Miner Res* **25**, 1468-1486
77. Rodriguez, S., Lei, X., Petersen, P. S., Tan, S. Y., Little, H. C., and Wong, G. W. (2016) Loss of CTRP1 disrupts glucose and lipid homeostasis. *Am J Physiol Endocrinol Metab* **311**, E678-E697
78. Schneider, C. A., Rasband, W. S., and Eliceiri, K. W. (2012) NIH Image to ImageJ: 25 years of image analysis. *Nat Methods* **9**, 671-675
79. Schmittgen, T. D., and Livak, K. J. (2008) Analyzing real-time PCR data by the comparative C(T) method. *Nat Protoc* **3**, 1101-1108
80. Sievers, F., and Higgins, D. G. (2018) Clustal Omega for making accurate alignments of many protein sequences. *Protein Sci* **27**, 135-145

FIGURE LEGENDS

Figure 1. TMEM263 is a novel and highly conserved plasma membrane protein. (A) Sequence alignment of full-length human (NP_689474), mouse (NP_001013046), chicken (NP_001006244), xenopus frog (NP_989399), and zebrafish (NP_998306) transmembrane protein 263 (TMEM263) using Clustal-omega (80). Identical amino acids are shaded black and similar amino acids are shaded grey. Gaps are indicated by dash lines. The two predicted transmembrane domains are indicated in red. (B) *TMEM263* expression across normal human tissues based on the consensus Human Protein Atlas (HPA) and Gene-Tissue Expression (GTeX) datasets. The data can be accessed via the HPA database (www.proteinatlas.org). nTPM denotes normalized protein-coding transcripts per million and it corresponds to the mean values of the different individual samples from each tissue. Bars are color-coded based on tissue groups with functional features in common. (C) Tmem263 expression across mouse tissues ($n = 11$). Relative expression across tissues were first normalized to *β-actin*, then normalize to the tissue (pancreas) with the lowest expression. (C) Immunoblot analysis of cell lysate from HEK293 cells transfected with a control pCDNA3 empty plasmid or plasmid encoding human TMEM263 tagged with a C-terminal Myc-DDK epitope. Immunoblots were probed with an anti-FLAG (DDK) antibody (left panel) or an anti-TMEM263 antibody (right panel). (D) TMEM263 is localized to the plasma membrane. Surface biotinylation was carried out on transfected HEK293 cells. Biotinylated plasma membrane proteins were captured with Avidin-agarose beads, eluted, and immunoblotted for TMEM263 with an anti-FLAG antibody.

Figure 2. Deletion of *Tmem263* gene causes dwarfism. (A) Generation of *Tmem263* knockout (KO) mice. The exon 3 that encodes ~81% of the full-length protein was deleted using CRISPR/Cas9 method and confirmed with DNA sequencing. The location and sequence of the two guide RNAs (gRNA) used to generate the deletion were underlined. Filled-in black boxes indicate part of the exon that codes for Tmem263 protein, and white boxes indicate part of the exon that codes for 5' and 3' UTR of the transcript. (B) Wild-type (WT) and KO alleles were confirmed by PCR genotyping. (C) The complete loss of *Tmem263* transcript in KO mice was confirmed by qPCR in male and female mouse liver and hypothalamus (WT, n = 6-8; KO, n = 6-8). (D) The expected Mendelian versus observed genotype distributions in P1 pups (n = 82). (E) Representative images of WT and *Tmem263*-KO pups at postnatal day 1 (P1). Milk spots are indicated by a red arrow. (F) Representative Alcian blue and Alizarin red staining of axial skeletal and

cartilage in WT and KO P1 pups. (G) Body weights of WT and *Tmem263*-KO pups at P1, P7, P14, and P21. (H) Representative images of adult WT and *Tmem263*-KO mice at 8 weeks of age. (I-J) Body weights and body length of WT (+/+), heterozygous (+/-), and KO (-/-) male and female mice at 8 weeks of age. (K) The growth curve trajectory based on the combined data in G and I. All data are presented as mean ± S.E.M. **** $P < 0.0001$ (One-way ANOVA with Tukey's multiple comparisons test).

Figure 3. Mice lacking TMEM263 exhibit pronounced skeletal dysplasia. (A) Representative microCT images of bone (femur) showing a dramatic reduction in size in *Tmem263* KO (-/-) mice relative to WT (+/+) and heterozygous (+/-) controls at 8 weeks of age. (B) Femur length of WT (+/+), heterozygous (+/-), and KO (-/-) male and female mice at 8 weeks of age. (C) Quantification of trabecular bone volume per tissue volume (BV/TV) in the distal femur of WT (+/+), heterozygous (+/-), and KO (-/-) mice. (D) Quantification of trabecular number (Tb. N) in the distal femur. (E) Trabecular bone thickness (Tb. Th). (F) Cortical tissue area (Tt. Ar). (G) Cortical area per tissue area. (H) Cortical thickness. (I) Tissue area per femur length. (J) Cortical thickness per femur length. (K) Representative images of tibial growth plate histology in WT and *Tmem263*-KO mice. (L-N) Quantification of growth plate length (L), proliferative zone length (M), and hypertrophic zone length (N) in WT ($n = 10$) and KO ($n = 10$) male mice. All data were collected on 8-week-old mice. All data are mean ± S.E. ** $P < 0.01$; *** $P < 0.001$; **** $P < 0.0001$ (One-way ANOVA with Tukey's multiple comparisons test).

Figure 4. TMEM263 deficiency results in marked reduction in circulating IGF-1, IGFBP3, and IGFALS levels. Serum levels of growth hormone (GH; A), IGF-1 (B), IGFBP3 (C), IGFALS (D), insulin (E), glucose (F), calcium (G), and phosphate (H) in WT (+/+), heterozygous (+/-) and *Tmem263*-KO (-/-) male and female mice at 8 weeks old. (I) Ratio of calcium-to-phosphate in WT, heterozygous, and KO male and female mice. All data are presented as mean ± S.E.M. * $P < 0.05$; ** $P < 0.01$; *** $P < 0.001$; **** $P < 0.0001$ (One-way ANOVA with Tukey's multiple comparisons test).

Figure 5. Reduced hepatic growth hormone receptor (GH-R) protein level and signaling in TMEM263 KO mice. (A) The GH/IGF-1 axis required for postnatal skeletal growth. At the onset of growth spurt, growth hormone releasing hormone (GHRH) from the hypothalamus causes the release of growth hormone (GH) from the anterior pituitary. Circulating GH binds to its receptor (GHR) in liver and other peripheral tissues to induce the synthesis and secretion of IGF-1, which then acts in an endocrine, paracrine, and/or autocrine manner to induce skeletal growth. (B) Expression levels of *Ghr* (growth hormone receptor), *Igf-1*, *Igfals* (IGF binding protein acid labile subunit), and *Igfbp3* (IGF binding protein 3) transcripts in the liver of WT and KO mice. Sample size of male mice (WT, $n = 8$; KO, $n = 8$) and Female mice (WT, $n = 8$; KO, $n = 8$). (C) Immunoblot analysis of growth hormone receptor (GH-R) protein levels in the liver of WT ($n = 7$) and KO ($n = 7$) mice. (D) Quantification of the immunoblot results as shown in C. (E) Reduced hepatic GH-induced signaling in KO (-/-) mice relative to WT (+/+) controls. Immunoblot analysis of phospho-JAK2 (Tyr1008), total JAK2, phospho-STAT5 (Y694), and total STAT5 in liver lysates from mice injected with recombinant GH. (F) Quantification of the immunoblot results as shown in E. All data are presented as mean ± S.E.M. ** $P < 0.01$; *** $P < 0.001$; **** $P < 0.0001$ (One-way ANOVA with Tukey's multiple comparisons test for data in B and two-tailed student's *t*-test for data in D and F).

Figure 6. Loss of TMEM263 disrupts GH-regulated gene expression in the liver. (A) Volcano plot of liver transcriptome. (B) Enrichment analysis of differentially expressed genes (DEGs) by Gene Ontology (GO), Kyoto Encyclopedia of Genes and Genomes (KEGG), and Reactome (http://www.reactome.org) databases. Plots of -Log(adj. p) vs gene ratio to show complete spread of all enrichment results for each analysis. The most effected categories are highlighted and labeled with the category name and number of up- and down-regulated genes within each. (C) Volcano plot showing the expression of all transcription factor (TF) genes detected in the liver transcriptome. TFs that are significantly up- or down-regulated in KO mouse liver are highlighted. (D) Heat map of DEGs involved in growth and metabolism. (E) Heat map of all protein-coding DEGs from the cytochrome P450 (Cyp) gene family. (F) Heat map of all protein-coding DEGs from the Major urinary protein (Mup) gene family. (G) Summary of key findings underpinning the dwarfism and skeletal dysplasia phenotypes of Tmem263-null mice. All heat map data is shown on a column z-score scale. Only significantly different genes (adjusted p-value < 0.05 and

Log_2(FC) <-1 or >1) are shown for all heat maps. PCG = protein coding gene, NPCG = non-protein coding gene. WT (n = 8) and KO (n = 8) for all data shown.

Supplemental Figure Legend

Figure 2 - figure supplement 1. Absolute and relative tissue and organ weights of *Tmem263* WT (+/+), heterozygous (+/-), and KO (-/-) male and female mice. The absolute weight of liver (A), pancreas (B), heart (C), kidney (D), spleen (E), skeletal muscle (gastrocnemius) (F), and brain (G) in WT, heterozygous, and KO mice. The relative weight, after normalization to body weight, of brain (H), liver (I), pancreas (J), heart (K), kidney (L), spleen (M), and gastrocnemius (N) in WT, heterozygous, and KO mice. All data are mean ± S.E. ** $P < 0.01$; *** $P < 0.001$; **** $P < 0.0001$ (One-way ANOVA with Tukey's multiple comparisons test).

Fig. 1

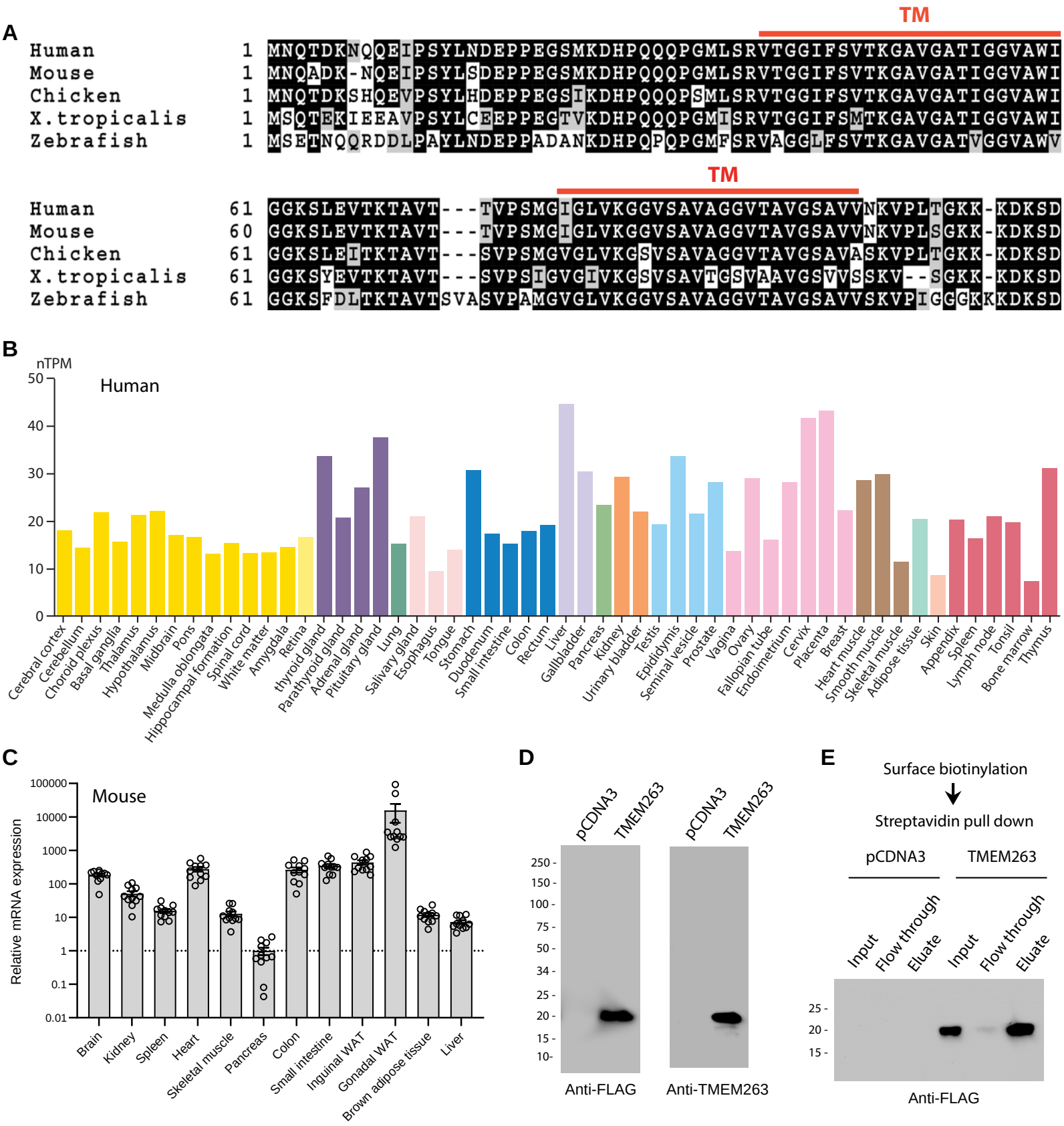
A
TM
Human 1 MNQTDKNQQEIPSYLNDEPPEGSMKDHPQQQPGMLSRVTGGIFSVTKGAVGATIGGVAWI
Mouse 1 MNQADK-NQEIPSYLSDEPPEGSMKDHPQQQPGMLSRVTGGIFSVTKGAVGATIGGVAWI
Chicken 1 MNQTDKSHQEVPSYLHDEPPEGSIKDHPQQQPSMLSRVTGGIFSVTKGAVGATIGGVAWI
X.tropicalis 1 MSQTEKIEEAVPSYLCEEPPEGTVKDHPQQQPGMISRVTGGIFSMTKGAVGATIGGVAWI
Zebrafish 1 MSETNQQRDDLPAYLNDEPPADANKDHPQPQPGMFSRVAGGLFSVTKGAVGATVGGVAWV
TM
Human 61 GGKSLEVTKTAVT---TVPSMGIGLVKGGVSAVAGGVTAVGSAVVNKVPLTGKK-KDKSD
Mouse 60 GGKSLEVTKTAVT---TVPSMGIGLVKGGVSAVAGGVTAVGSAVVNKVPLSGKK-KDKSD
Chicken 61 GGKSLEITKTAVT---SVPSMGVGLVKGSVSAVAGGVTAVGSAVASKVPLTGKK-KDKSD
X.tropicalis 61 GGKSYEVTKTAVT---SVPSIGVGIVKGSVSAVTGSVAAVGSVVSSKV--SGKK-KDKSD
Zebrafish 61 GGKSFDLTKTAVTSVASVPAMGVGLVKGGVSAVAGGVTAVGSAVVSKVPIGGGKKKDKSD
B
nTPM
Human
50
40
30
20
10
0
Cerebral cortex
Cerebellum
Choroid plexus
Basal ganglia
Thalamus
Hypothalamus
Midbrain
Pons
Medulla oblongata
Hippocampal formation
Spinal cord
White matter
Amygdala
Retina
thyroid gland
Parathyroid gland
Adrenal gland
Pituitary gland
Lung
Salivary gland
Esophagus
Tongue
Stomach
Duodenum
Small intestine
Colon
Rectum
Liver
Gallbladder
Pancreas
Kidney
Urinary bladder
Testis
Epididymis
Seminal vesicle
Prostate
Vagina
Ovary
Fallopian tube
Endoimetrium
Cervix
Placenta
Breast
Heart muscle
Smooth muscle
Skeletal muscle
Adipose tissue
Skin
Appendix
Spleen
Lymph node
Tonsil
Bone marrow
Thymus
C
Mouse
Relative mRNA expression
100000
10000
1000
100
10
1
0.1
0.01
Brain
Kidney
Spleen
Heart
Skeletal muscle
Pancreas
Colon
Small intestine
Inguinal WAT
Gonadal WAT
Brown adipose tissue
Liver
D
pCDNA3
TMEM263
pCDNA3
TMEM263
250 -
150 -
100 -
75 -
50 -
34 -
25 -
20 -
15 -
10-
Anti-FLAG
Anti-TMEM263
E
Surface biotinylation
Streptavidin pull down
pCDNA3
TMEM263
Input
Flow through
Eluate
Input
Flow through
Eluate
25 -
20 -
15 -
Anti-FLAG

Fig. 2

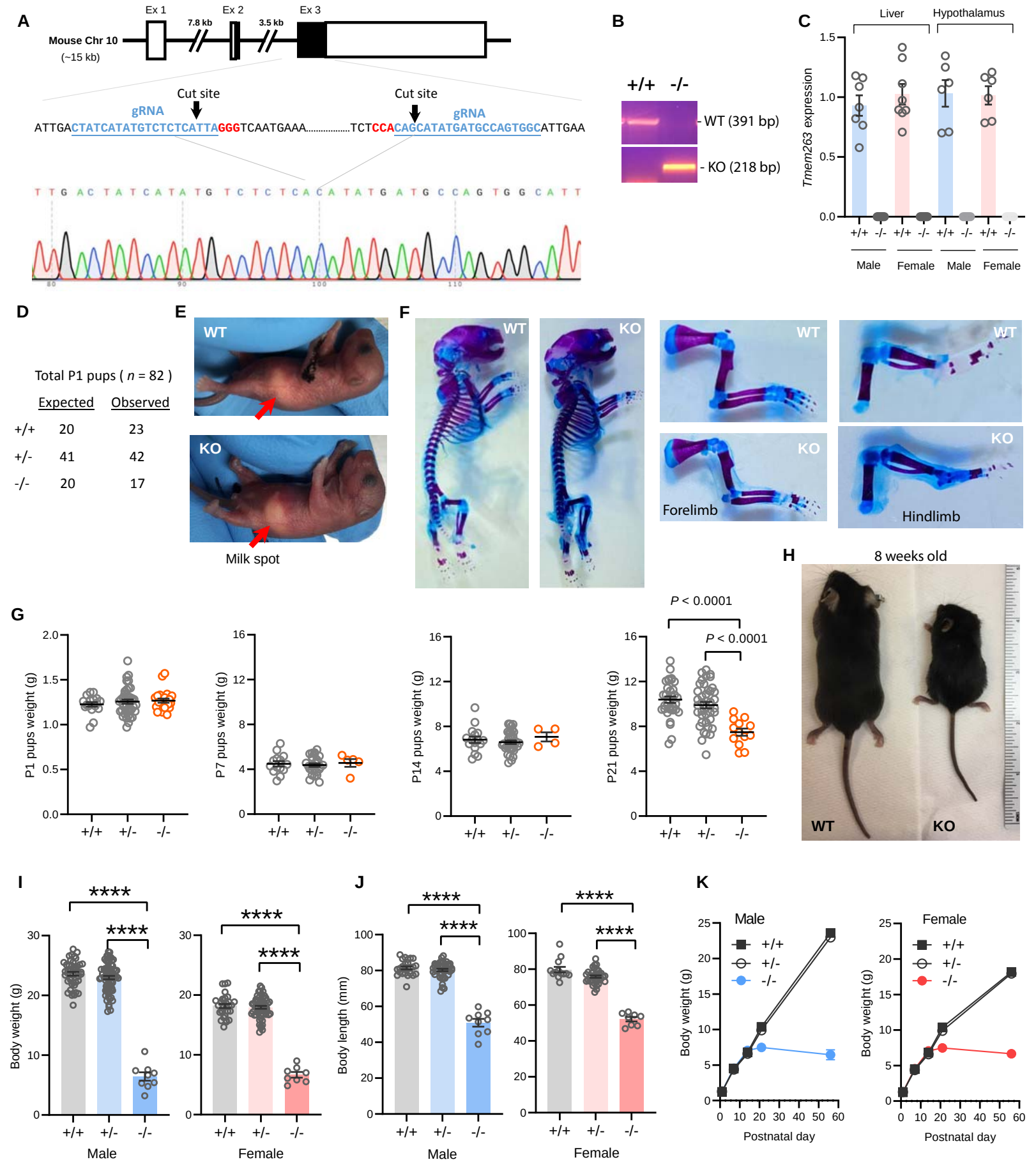
A
Mouse Chr 10
(~15 kb)
Ex 1
Ex 2
Ex 3
7.8 kb
3.5 kb
Cut site
gRNA
ATTGACTATCATATGTCTCTCATTAGGGTCAATGAAA.....TCTCCACAGCATATGATGCCAGTGGCATTGAA
B
+/+ -/-
- WT (391 bp)
- KO (218 bp)
C
Liver
Hypothalamus
Tmem263 expression
Male
Female
D
Total P1 pups (n = 82)
Expected Observed
+/+ 20 23
+/- 41 42
-/- 20 17
E
WT
KO
Milk spot
F
WT
KO
Forelimb
Hindlimb
G
P1 pups weight (g)
P7 pups weight (g)
P14 pups weight (g)
P21 pups weight (g)
P < 0.0001
P < 0.0001
H
8 weeks old
WT
KO
I
Body weight (g)
Male
Female
J
Body length (mm)
Male
Female
K
Male
Female
Body weight (g)
Postnatal day

Fig. 3

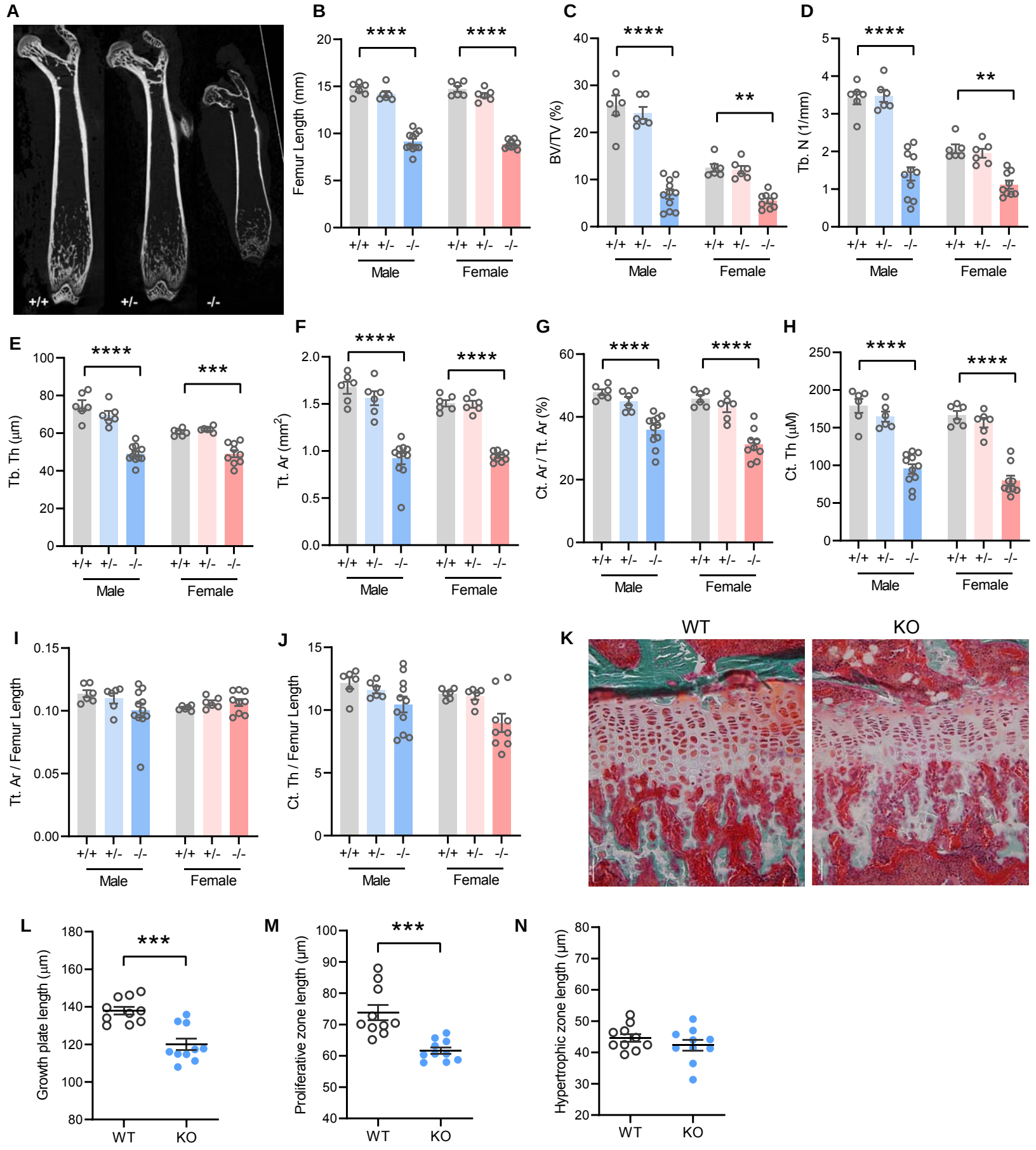
A
+/+
+/-
-/-
B
Femur Length (mm)
C
BV/TV (%)
D
Tb. N (1/mm)
E
Tb. Th (μm)
F
Tt. Ar (mm2)
G
Ct. Ar / Tt. Ar (%)
H
Ct. Th (μM)
I
Tt. Ar / Femur Length
J
Ct. Th / Femur Length
Male
Female
K
WT
KO
L
Growth plate length (μm)
M
Proliferative zone length (μm)
N
Hypertrophic zone length (μm)

Fig. 4

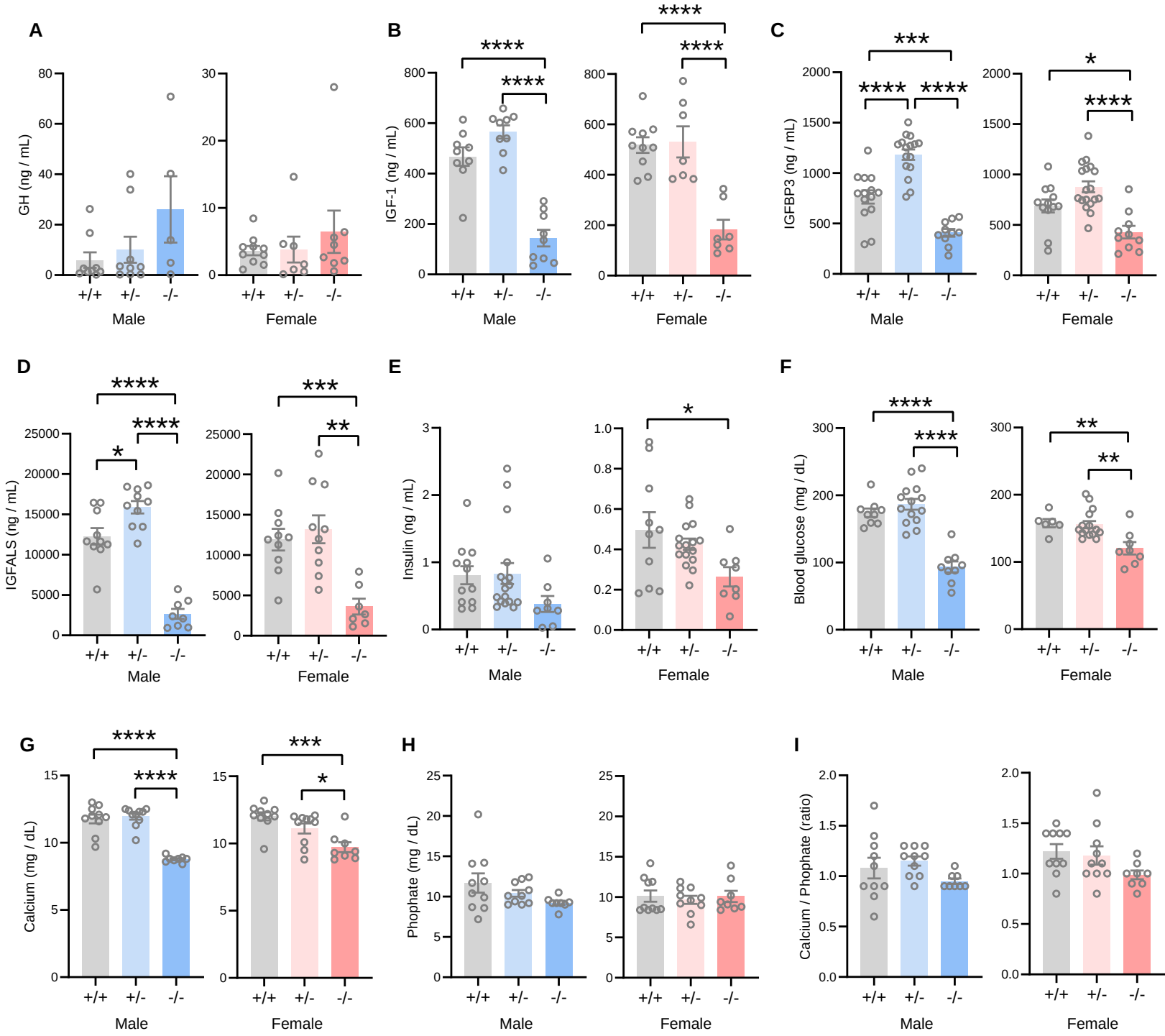
A
GH (ng / mL)
Male
Female
B
IGF-1 (ng / mL)
C
IGFBP3 (ng / mL)
D
IGFALS (ng / mL)
E
Insulin (ng / mL)
F
Blood glucose (mg / dL)
G
Calcium (mg / dL)
H
Phophate (mg / dL)
I
Calcium / Phophate (ratio)
+/+
+/-
-/-

Fig. 5

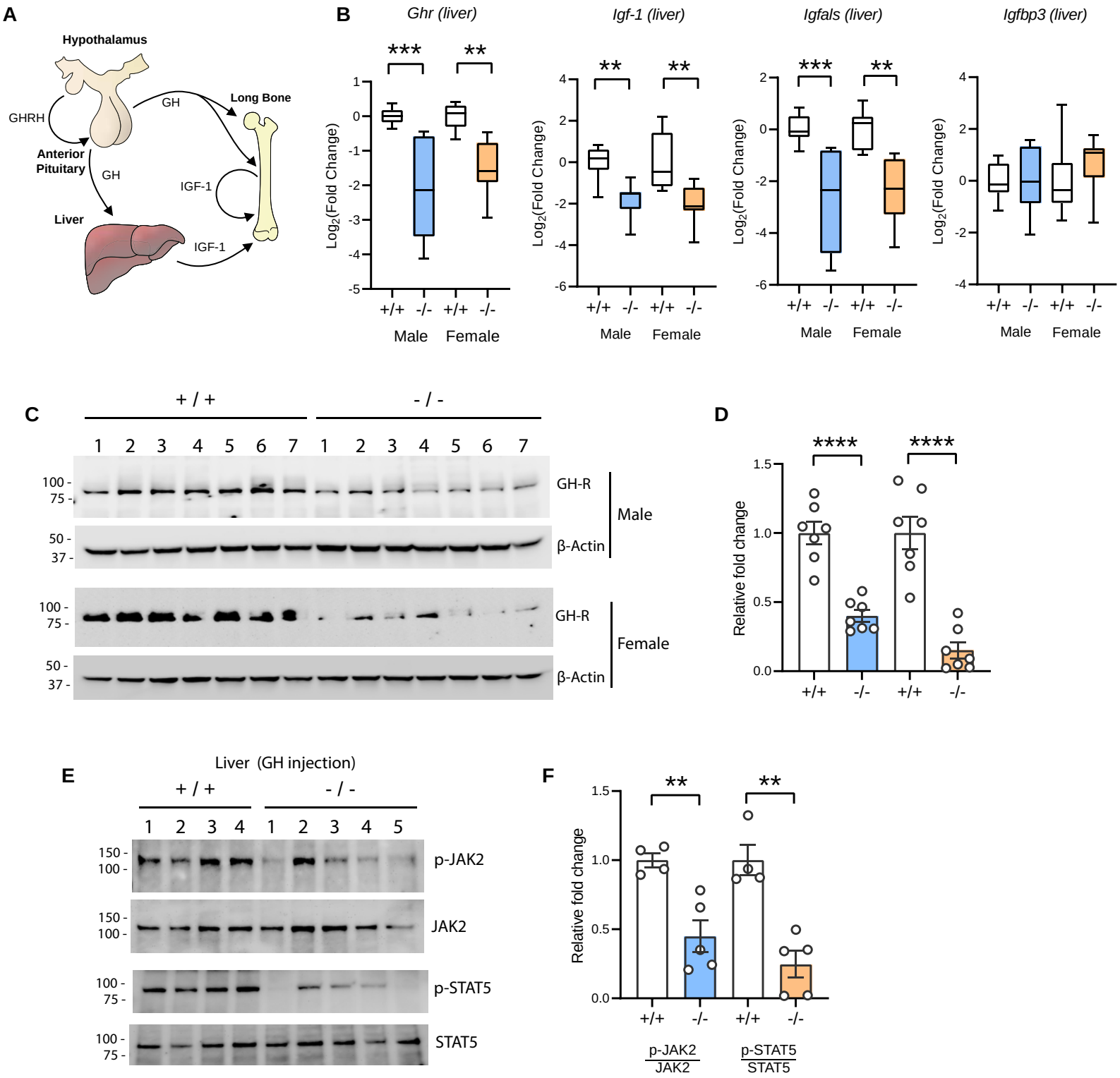
A
Hypothalamus
GHRH
GH
Long Bone
Anterior Pituitary
GH
IGF-1
Liver
IGF-1
B
Ghr (liver)
Igf-1 (liver)
Igfals (liver)
Igfbp3 (liver)
Log2(Fold Change)
+/+ -/- +/+ -/-
Male Female
C
+ / +
- / -
1 2 3 4 5 6 7 1 2 3 4 5 6 7
100 -
75 -
50 -
37 -
GH-R
β-Actin
Male
Female
D
Relative fold change
+/+ -/- +/+ -/-
E
Liver (GH injection)
+ / +
- / -
1 2 3 4 1 2 3 4 5
150 -
100 -
75 -
p-JAK2
JAK2
p-STAT5
STAT5
F
Relative fold change
+/+ -/- +/+ -/-
p-JAK2 / JAK2
p-STAT5 / STAT5

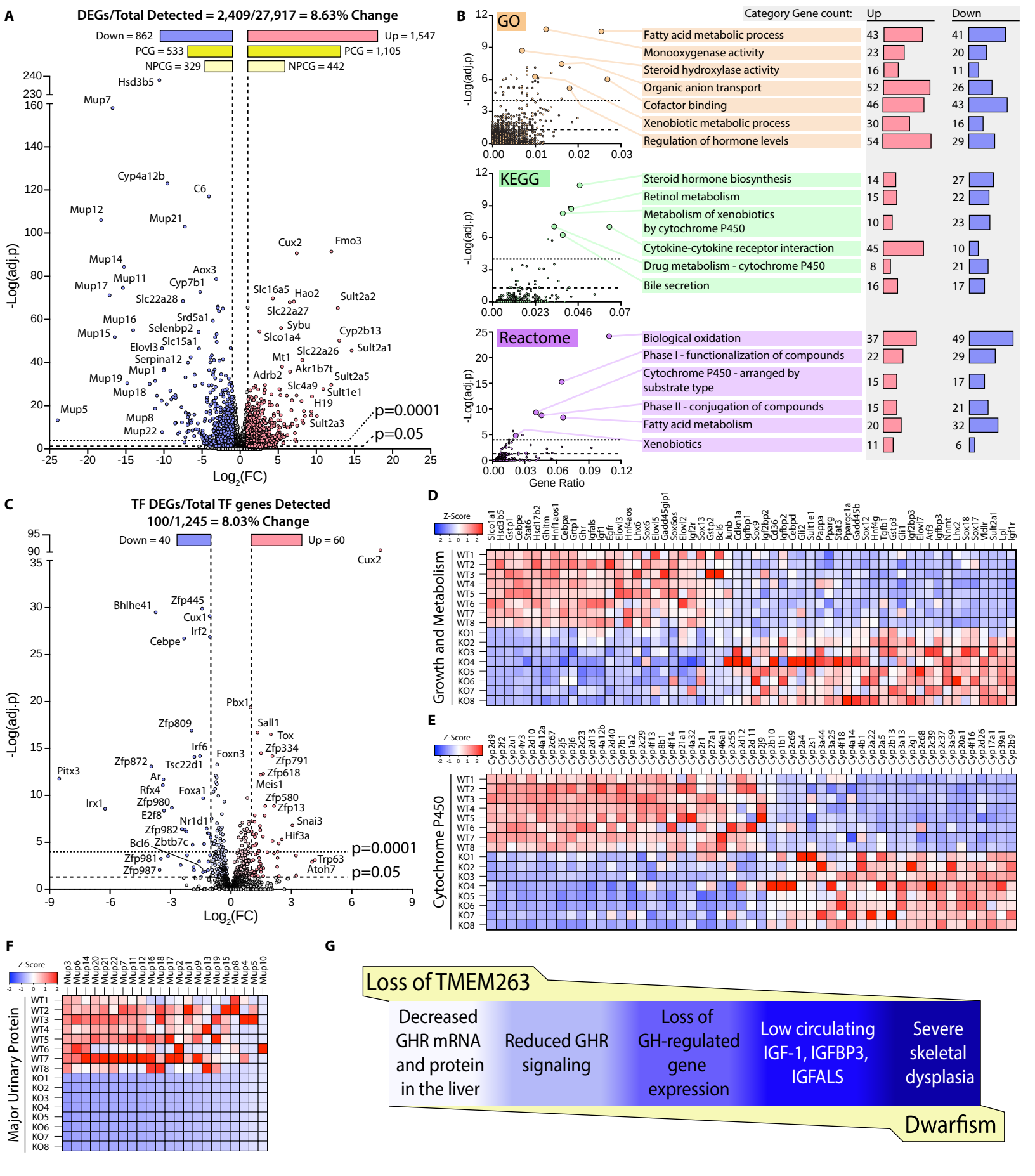
A
DEGs/Total Detected = 2,409/27,917 = 8.63% Change
Down = 862
Up = 1,547
PCG = 533
PCG = 1,105
NPCG = 329
NPCG = 442
-Log(adj.p)
Log2(FC)
p=0.0001
p=0.05
B
GO
KEGG
Reactome
Category Gene count:
Up
Down
Fatty acid metabolic process 43 41
Monooxygenase activity 23 20
Steroid hydroxylase activity 16 11
Organic anion transport 52 26
Cofactor binding 46 43
Xenobiotic metabolic process 30 16
Regulation of hormone levels 54 29
Steroid hormone biosynthesis 14 27
Retinol metabolism 15 22
Metabolism of xenobiotics by cytochrome P450 10 23
Cytokine-cytokine receptor interaction 45 10
Drug metabolism - cytochrome P450 8 21
Bile secretion 16 17
Biological oxidation 37 49
Phase I - functionalization of compounds 22 29
Cytochrome P450 - arranged by substrate type 15 17
Phase II - conjugation of compounds 15 21
Fatty acid metabolism 20 32
Xenobiotics 11 6
Gene Ratio
C
TF DEGs/Total TF genes Detected
100/1,245 = 8.03% Change
Down = 40
Up = 60
p=0.0001
p=0.05
D
Growth and Metabolism
Z-Score
E
Cytochrome P450
F
Major Urinary Protein
G
Loss of TMEM263
Decreased GHR mRNA and protein in the liver
Reduced GHR signaling
Loss of GH-regulated gene expression
Low circulating IGF-1, IGFBP3, IGFALS
Severe skeletal dysplasia
Dwarfism

Fig. 6